Global analysis of surface ocean CO2 fugacity and air-sea fluxes with low latency

Thi-Tuyet-Trang Chau[1], Frederic Chevallier[2], and Marion Gehlen[3]

[1]Laboratoire des Sciences du Climat et de l'Environnement
[2]Laboratoire des Sciences du Climat et de l'Environnement (LSCE)
[3]LSCE

October 14, 2023

Abstract

The Surface Ocean CO2 Atlas (SOCAT) of CO2 fugacity (fCO2) observations is a key resource supporting annual assessments of CO2 uptake by the ocean and its side effects on the marine ecosystem. SOCAT data are usually released with a lag of up to 1.5 years which hampers timely quantification of recent variations of carbon fluxes between the Earth System components, not only with the ocean. This study uses a statistical ensemble approach to analyse fCO2 with a latency of one month only based on the previous SOCAT release and a series of predictors. A retrospective prediction for the years 2021-2022 is made to test the model skill, followed by the generation of fCO2 and fluxes from January to August in 2023. Results indicate a modest degradation of the model skill in prediction mode and open the possibility to provide robust information about marine carbonate system variables with low latency.

Global analysis of surface ocean CO_2 fugacity and air-sea fluxes with low latency

Thi-Tuyet-Trang Chau[1], Frédéric Chevallier[1], and Marion Gehlen[1]

[1]Laboratoire des Sciences du Climat et de l'Environnement, LSCE/IPSL, CEA-CNRS-UVSQ, Université Paris-Saclay, F-91191 Gif-sur-Yvette, France

Key Points:

- We demonstrate the capacity of statistical models to generate global maps of $f CO_2$ and air-sea flux with a latency reduced to one month.
- A decrease in the CO_2 source for January to August 2023 diagnosed in the tropical Pacific coheres with the retreat of the La Niña event.
- An unusual northeastern Atlantic sink reduction diagnosed for June 2023 is linked to record heat and exceptionally low winds.

Corresponding author: Thi-Tuyet-Trang Chau, thi.tuyet.trang.chau@gmail.com

Abstract

The Surface Ocean CO_2 Atlas (SOCAT) of CO_2 fugacity ($f CO_2$) observations is a key resource supporting annual assessments of CO_2 uptake by the ocean and its side effects on the marine ecosystem. SOCAT data are usually released with a lag of up to 1.5 years which hampers timely quantification of recent variations of carbon fluxes between the Earth System components, not only with the ocean. This study uses a statistical ensemble approach to analyse $f CO_2$ with a latency of one month only based on the previous SOCAT release and a series of predictors. A retrospective prediction for the years 2021-2022 is made to test the model skill, followed by the generation of $f CO_2$ and fluxes from January to August in 2023. Results indicate a modest degradation of the model skill in prediction mode and open the possibility to provide robust information about marine carbonate system variables with low latency.

Plain Language Summary

There is a growing need to monitor carbon emissions and removals over the globe in near real time in order to correctly interpret changes in CO_2 concentrations as they unfold. For the oceans, the best information comes from measurements of the surface ocean CO_2 fugacity ($f CO_2$) by the international marine carbon research community. So far, this data is mostly available 6 to 18 months behind real time after collection, qualification, harmonization, and processing. Here, we show that a set of biological, chemical, and physical predictors available in near-real time, allows the information contained in the "old" $f CO_2$ measurements to be transferred over time. Based on a statistical technique, we combine all these data sources to estimate global monthly maps of $f CO_2$ and of CO_2 fluxes at the air-sea interface within one month behind real time and with good accuracy.

1 Introduction

The ocean is a sink taking up about 26% of atmospheric carbon dioxide (CO_2) and 90% of the heat-induced largely by anthropogenic greenhouse gas emissions (Canadell et al., 2021; Friedlingstein et al., 2022). A side effect of the ocean's role as a global climate modulator is the increase in seawater acidity, which dramatically affects marine ecosystems (Hopkins et al., 2020; Doney et al., 2020; Cooley et al., 2022). The global ocean carbon sink is proportional to CO_2 human emissions only at the decadal scale. On shorter time scales, it varies with the climate (mostly temperature and winds), with a dependency that also varies from basin to basin given their respective geographical, dynamic, and biological specificities (Rödenbeck et al., 2015; Landschützer et al., 2016; Gruber et al., 2023).

Measurements of surface ocean CO_2 fugacity (fCO_2) from ships, drifters, moorings, and autonomous surface platforms are the main reference to document the actual variation of air-sea fluxes ($fgCO_2$) in space and time (Friedlingstein et al., 2022) because the two are linearly related. Long-term efforts in maintaining and expanding international observing networks together with a coordinated data aggregation of the Surface Ocean CO_2 Atlas database - SOCAT (Bakker et al., 2016, 2023) have provided millions of individual fCO_2 observations since the 1950s and associated gridded products. However, fCO_2 data are poorly sampled leaving out most areas for some or all of the year. Statistical data-based reconstructions of fCO_2 (Rödenbeck et al., 2013; Landschützer et al., 2016; Gregor & Gruber, 2021; Chau et al., 2022b) have emerged to gap-fill the SOCAT database using auxiliary data, resulting in reconstructions of fCO_2 global monthly maps. They are still the topic of active research to improve the reconstruction quality, but these maps lag behind real time by 0.5 to 1.5 years: the update of the SOCAT archive follows an annual pace with a public release usually in June after measurement collection, quality control, and processing. This lag is problematic for the documentation of the carbon cycle as it evolves, while the main variables of the carbon cycle are progressively integrated within operational programmes with much faster data releases. A prominent example of operational programmes in need of a reduced time lag is the operational observation-based anthropogenic CO_2 emissions monitoring and verification support capacity (CO_2MVS) that the European Commission is building under its Copernicus Earth Observation programme (e.g., Janssens-Maenhout et al. (2020)). As its observational component relies heavily on satellite observations of CO_2 in the atmosphere, which is affected by the ocean as well as terrestrial emissions and removals, better estimates of fCO_2 would result in efficient estimates of air-sea fluxes and thence benefit air-land flux accuracy, in addition to being directly interesting to users. The CO_2MVS fits within the Global Greenhouse Gas Watch, an even larger greenhouse gas monitoring infrastructure that the World Meteorological Organization (WMO) is setting up (`https://public.wmo.int/en/media/press-release/world-meteorological-congress-approves-global-greenhouse-gas-watch`, last access: 20/9/2023).

Here, we demonstrate the capability to retrieve global monthly maps of fCO_2 from SOCAT data and then to generate the corresponding fields of air-sea fluxes with a lag reduced to one month. To do that, we extend the work of Chau et al. (2022b) who have been gap-filling SOCAT gridded data within the framework of the Copernicus Marine Environment Monitoring Service (CMEMS) based on an ensemble of feed-forward neural network models (also referred to as CMEMS-LSCE-FFNN) and a set of biological, chemical, and physical predictors. While Chau et al. (2022b) made the dates of the predictors and the date of the gridded SOCAT data coincide, we turn to a prediction mode in which the relationship found between the predictors and the SOCAT data more than 6 months before is kept. Section 2 below describes the method. We test the approach in the years 2021-2022 by examining the retrospective prediction skill based on the available SOCAT data. Then we expand model prediction of $f\mathrm{CO_2}$ and generate $fg\mathrm{CO_2}$ up to present with a latency of 1 month: data access via the Institut Pierre-Simon Laplace (LSCE/IPSL) data center, `https://dods.lsce.ipsl.fr/invsat/FFNN_low-latency/`. The results include the finding of anomalous variations in regional $\mathrm{CO_2}$ uptake and release by the ocean predicted in January to August 2023, as described in Section 3. Section 4 draws the main conclusions of the study.

2 Materials and Methods

CMEMS-LSCE-FFNN (Chau et al., 2022b) is built on machine-learning techniques. It consists of an ensemble of feed-forward neural network (FFNN) models. This ensemble approach was developed at LSCE in order to reconstruct surface ocean carbonate system variables and to support the operational distribution of such datasets by CMEMS since 2019 (Product identity: MULTIOBS_GLO_BIO_CARBON_SURFACE_REP_015_008, `https://doi.org/10.48670/moi-00047`, last access: 22/9/2023). The CMEMS-LSCE-FFNN fields cover the global ocean at a resolution of $1^\circ \times 1^\circ$ currently and for the period since the year 1985 at monthly resolution.

Under the hood, these FFNN models represent nonlinear mappings of $f\mathrm{CO_2}$ against a set of predictors. Monthly gridded observation-based products of $f\mathrm{CO_2}$ from SOCAT (Bakker et al., 2016) are used as the target data in model fitting. $f\mathrm{CO_2}$ predictors are environmental variables: sea surface temperature (SST), sea surface salinity (SSS), sea surface height (SSH), chlorophyll-a (Chl-a), mix-layer-depth (MLD), $\mathrm{CO_2}$ surface mole fractions ($x\mathrm{CO_2}$), climatological $f\mathrm{CO_2}$ ($f\mathrm{CO_2}^{\mathrm{clim}}$), and geographical coordinates (latitude and longitude). Product resources of input datasets are detailed in Table S1. CMEMS-LSCE-FFNN comprises monthly adaptive FFNN models for which the $f\mathrm{CO_2}$ and predictor datasets available within a time span of 3 months for all the years since 1985 (the reconstruction month excepted) are used in the fitting phase. SOCAT fCO_2 in the reconstruction month is only used in model evaluation. The ensemble of multi-FFNN models was designed by randomly splitting two-thirds of the 3-month sliding datasets for training and the rest for model test (Chau et al., 2022b). From the ensemble reconstructions, the model best estimate (ensemble mean) and 1σ - model uncertainty (ensemble standard deviation) of fCO_2 are derived at the desired resolution.

Here we revisit the two versions of CMEMS-LSCE-FFNN referred to as FFNNv2021 and FFNNv2022. These two models respectively used SOCATv2021 and SOCATv2022 datasets (Bakker et al., 2021, 2022) as the target input data of fCO_2. Note that SOCAT has been annually published mid-June. Due to the delay mode for data collection, reprocessing, and qualify control, SOCAT provides gridded data up to the year before the publication date (see Bakker et al. (2016, 2023) for instance). For the period 1985-2021, SOCATv2022 offers an amount of roughly 311700 monthly 1-degree gridded data, 5000 more than SOCATv2021 (Table S3a). The data increase in SOCATv2022 is mostly distributed within the last three years due to the late availability of some data sources (Figure 1). However, SOCATv2021 has more data before 2018, up to at least 1000 more in some years (e.g., 2011 and 2012) due to an erroneous flagging of some data (Bakker et al., 2021). Despite this feature, the two corresponding FFNN reconstructions do not exhibit large systematic offsets in their fCO_2 estimates (Chau et al., 2022a).

For all experiments in this study, the ensemble size (i.e., number of FFNN model runs) is set to 50. FFNN with 50 ensemble members has less computational complexity than with the usual size of 100 but it shows similar reconstruction skill (Chau et al. (2022b); Figure S2). The same input data of predictors is fed to the two FFNN model runs (Table S1). The FFNNv2021 (respectively FFNNv2022) model relies on SOCATv2021 (respectively SOCATv2022) and predictor datasets in 1985-2020 (respectively 1985-2021). This allows deriving the ensemble global reconstructions of fCO_2 over the 36-year and 37-year periods, accordingly. The ensemble of FFNN models is then applied to predict fCO_2 given the set of predictors in the years 2021-2022 for version 2021 and in the year 2022 for the latter. The quality assessments are made for (1) the two global reconstructions in the period 1985-2020, (2) FFNNv2021 one-year prediction against FFNNv2022 one-year reconstruction in 2021, and (3) FFNNv2021 two-year prediction against FFNNv2022 one-year prediction in 2022. Model performances will be qualified with the latest SOCAT data, i.e., SOCATv2023 (Bakker et al., 2023). The number of evaluation data for prediction in the years 2021 and

2022 over the global ocean is 10908 and 8602, respectively (Table S3a), which is statistically sufficient for significant validation.

Model skills are examined from global to sub-basin scale. Here we consider the sub-basins defined by the REgional Carbon Cycle Assessment and Processes2 project (`https://github.com/RECCAP2-ocean/RECCAP2-shared-resources/tree/master/data/regions`, last access: 20/3/2023). Due to a lack of evaluation data in several RECCAP2 biomes, we aggregate some of them, yielding 14 provinces in total (see Table S2 and Figure S1). These ocean provinces, therefore, differ from the original biomes proposed by Fay and McKinley (2014). Apart from the Northern Indian Ocean (11.NIO), the number of data for prediction evaluation ranges from 133 (12.SIO, i.e., Southern Indian Ocean) to 2350 (2.NA-SS, i.e., North Atlantic seasonally stratified) in the year 2021 and from 73 to 2265 in the year 2022.

For the actual prediction in 2022 and 2023, the latest model (FFNNv2022) has been run given monthly data of predictors (Table S1) in the year 2022 to present. We choose to release the maps of $f\mathrm{CO_2}$ and $fg\mathrm{CO_2}$ for the previous month on the 15th of each month.

3 Evaluation and Discussions

3.1 Reconstruction and Prediction of $\mathbf{CO_2}$ fugacity in 1985-2022

3.1.1 Global qualification

FFNNv2021 and FFNNv2022 share consistent global RMSD and determination coefficient r^2 (Figure 1 and Table S3). Between 1985 and 2020, the two reconstructions inherit the same RMSD of 19.1 μatm and r^2 of 0.78 (Table S3b). Improvement in the global reconstruction skill of FFNNv2022 in recent years (Figure 1b) is moderate despite 5000 additional $f\mathrm{CO_2}$ data in the model training (Figure 1a). In detail, these 1.7% additional data in SOCATv2022 (311694 in total) in 1985-2021 correspond to 9615 data added in 2021 and 4278 data removed from SOCATv2021 in 1985-2020 (see the spatial distribution of removal data in Figure S2c).

The RMSD variability before 2018 (Figure 1b) is likely linked to changes in the data sampling in regions with high spatiotemporal variability of $f\mathrm{CO_2}$ (see Gregor et al. (2019); Chau et al. (2022b) for further analysis). However, the difference between the RMSD of the two reconstructions is negligible then, as it fluctuates within $[-0.1, 0.1]$ μatm. During the last four years, a monotonous increase in RMSD (Figure 1b) coexists with a decrease in

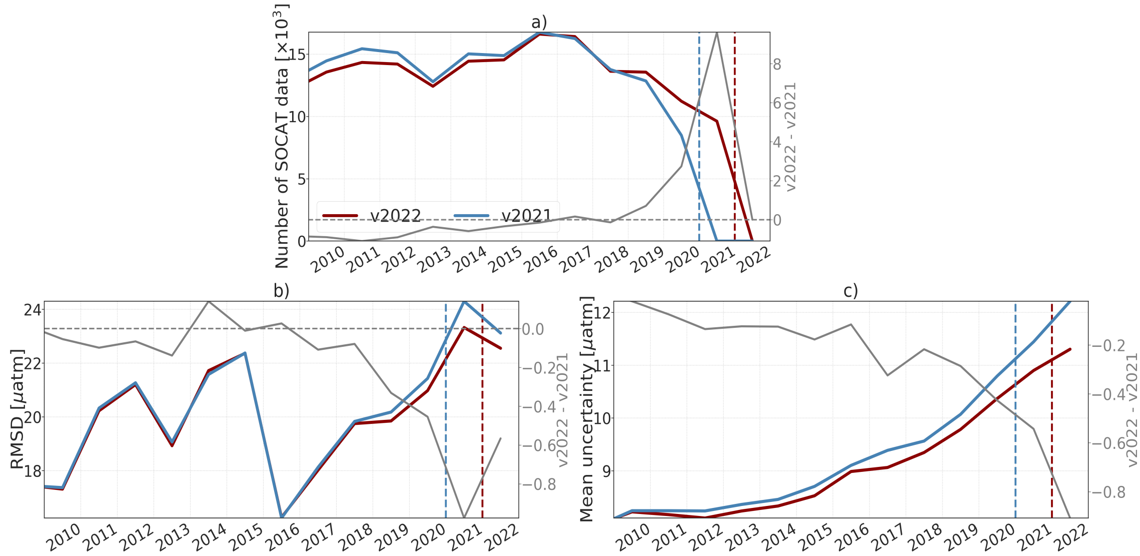

Figure 1. (a) Number of data per year in SOCATv2021 and SOCATv2022, (b) RMSD of FFNNv2021 and FFNNv2022 against SOCATv2023 fCO_2, (c) yearly global mean uncertainty (1σ). Differences between the two versions are shown with a grey solid curve with values on the right y-axis whereas the grey solid curve below 0 (grey dashed horizontal line). The blue and red vertical lines mark the start of the prediction mode for FFNNv2021 and FFNNv2022, respectively.

the number of SOCAT data (Figure 1a), and the FFNNv2021 reconstruction slightly, but increasingly, underperforms compared to FFNNv2022. In 2021 and 2022, the FFNNv2021 prediction RMSD is 24.3 μatm and 23.1 μatm, respectively, roughly $0.5-1$ μatm higher than that of the FFNNv2022 reconstruction and prediction (Table S3). Likewise, the variation of SOCAT fCO_2 is reproduced with high r^2 values (0.74 and 0.75), close to the one-year reconstruction and prediction of FFNNv2022 (0.76) for the years 2021-2022.

The yearly-mean uncertainty over the global ocean (Figure 1c) is computed by weighting the model estimated uncertainty (ensemble spread) per grid cell (σ) with the geographical area. The two reconstructions before the year 2015 are rather stable with an uncertainty about 8.5 μatm. The increase in FFNNv2021 [v2022] model uncertainty from 8.7 μatm [8.5 μatm] to 10.8 μatm [10.4 μatm] between 2015-2020 follows a decrease in observation-based data from 14877 [14533] to 8482 [11217] (Figure 1a). In the year 2021, the FFNNv2021 uncertainty of predicted fCO_2 (11.4 μatm) is slightly higher than that of the FFNNv2022 reconstruction but the offset between the two values is as small as 0.5 μatm (Figure 1c). The prediction uncertainty in 2022 increases by $0.4 - 0.8$ μatm for the two models (FFNNv2021: 12.2 μatm, FFNNv2022: 11.3 μatm).

3.1.2 Regional assessment

Model reconstruction and prediction skills are assessed over 14 ocean provinces (Figure S1 and Table S2) in the years 1985-2020 and 2021-2022 (1985-2021 and 2022) for FFNNv2021 (FFNNv2022). Results of the regional evaluation are summarized in Figure 2 and Table S4. The two FFNN models perform with a similar skill in reconstruction mode (1985-2020) over all ocean provinces. Evidently, their reconstructions share consistent patterns in regional-mean fCO_2 (Figure 2b) and in the spatial and temporal variations (Figures S4abc and S7) with systematic biases below 1 μatm for most of the basins (Table S4). Differences in uncertainty estimates and RMSD do not exceed 0.5 μatm while those in r^2 are nearly the same (Figure 2cde and Table S4).

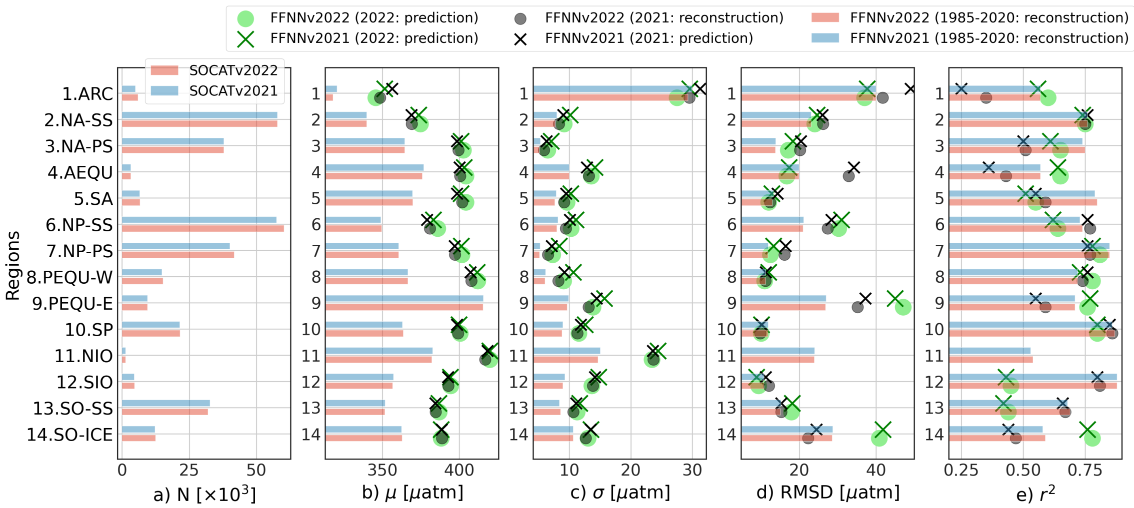

Figure 2. Regional comparisons of the two FFNN reconstructions in 1985-2020 (bars) and of the FFNNv2021 prediction versus the FFNNv2022 reconstruction [prediction] in 2021 [2022] (objects) in terms of (a) N- number of SOCAT monthly gridded data used in model fitting, (b) μ- mean fCO_2, (c) σ-mean uncertainty, (d) RMSD model-data deviation, and (e) r^2 model-data correlation.

In the years 2021-2022, RMSD (r^2) of the FFNN prediction does not change from the full-period reconstruction by more than about 5 μatm (0.1) over many sub-basins (e.g., 2.NA-SS, 7.NP-PS, 8.PEQU-W, 10.SP, 12.SIO, and 13.SO-SS). As expected, FFNNv2022 (one-year prediction) performs slightly better than FFNNv2021 (two-year prediction) in the

2022 prediction for many regions (Figures 2de and Table S4). However, the differences in regional skill scores of the two models are substantially small, i.e., below 3 μatm for RMSD and 0.05 for r^2. These results suggest a high confidence level in FFNN prediction for a few years ahead. The analysis of the spatial distribution and of the time series (Figures 2, S4, and S7) also reveals consistent features (horizontal gradients of $f\mathrm{CO_2}$ and seasonality to long-term variations) from the reconstruction years to the prediction years. $f\mathrm{CO_2}$ increases over time (see f.i., 7.NP-PS, 8.PEQU-W, 12.SIO) following the trend in atmospheric $\mathrm{CO_2}$ concentration. Among the $f\mathrm{CO_2}$ predictors, $x\mathrm{CO_2}$ stands out with its large increasing trend that brings some $x\mathrm{CO_2}$ data used in the prediction above the range of those used in the training. The growth of atmospheric $\mathrm{CO_2}$ is the primary factor driving the increase in sea surface $f\mathrm{CO_2}$ (Bates et al., 2014; Gruber et al., 2019; Landschützer et al., 2019; Friedlingstein et al., 2022). The prediction skill, however, does not degrade compared to the reconstruction as the annual increment of $f\mathrm{CO_2}$ is typically smaller than its intra-annual variability (Figure S6). The latter is dominantly driven by temperature-dependent $\mathrm{CO_2}$ solubility and biological processes (Takahashi et al., 2002; Gallego et al., 2018; Rustogi et al., 2023). The range of the pre-2021 [pre-2022] training datasets of physical and biological predictors (e.g., SST, Chl-a) remains similar to that including input data in the next year, seasonality to multi-month variations of $f\mathrm{CO_2}$ in the years 2021-2022 can be, therefore, propagated with these covariates overall. The majority of SOCAT $f\mathrm{CO_2}$ data for 2021 [2022] stays within the full range of training data which also supports FFNNs to achieve a skillful prediction (Figure S3). Further analysis of FFNN prediction skills over ocean basins is presented in the Supporting Information document.

3.2 Prediction of air-sea $\mathbf{CO_2}$ fluxes in 2022-2023

The previous results emphasize the skill and reliability of FFNN models in both reconstruction and prediction of $\mathrm{CO_2}$ fugacity ($f\mathrm{CO_2}$). In this section, we will use the FFNNv2022 predicted $f\mathrm{CO_2}$ field to generate corresponding air-sea fluxes ($fg\mathrm{CO_2}$) and analyze preliminary results for 20 months, from January 2022 to August 2023. $fg\mathrm{CO_2}$ is given in molC.m^{-2}.yr^{-1} for a flux density and in PgC.yr^{-1} for integration over ocean basins (see Supporting Information for details of flux calculation and analysis). FFNNv2022 predicts a reduction in the global ocean uptake of $\mathrm{CO_2}$ for 2022 (2.25 ± 0.5 PgC.yr^{-1}) compared to the previous year (2.36 ± 0.43 PgC.yr^{-1}). When adjusting the estimated global net fluxes with the riverine outgassing of $\mathrm{CO_2}$ of 0.65 PgC.yr^{-1} (Regnier et al., 2022) and the total ocean surface area (FFNNv2022 data covers 95% of the global ocean), one obtains the estimates of anthropogenic ocean carbon uptake consistent with the 2022 projection proposed by Friedlingstein et al. (2022): the anthropogenic ocean sink in 2021 was 2.9 ± 0.4 PgC.yr^{-1} remains unchanged for the year 2022. This evidence supports their hypothesis that the persistence of cooling climate patterns (La Niña conditions) weakened CO_2 ocean uptake in 2021-2022 (high peaks appeared mid-2022, Figure S9). FFNNv2022 predicts a global net flux of 2.45 ± 0.56 PgC.yr^{-1} for January to August 2023, the enhancement of global ocean uptake compared to that in 2022 (2.17 ± 0.50 PgC.yr^{-1}) is synchronous with the retreat of La Niña.

The model prediction retains the seasonal to interannual variations of $f\mathrm{CO_2}$ and $fg\mathrm{CO_2}$ in the pre-2022 reconstruction over many ocean basins (Figures S6 and S8). One of the remarkable changes is observed at the equatorial Atlantic (4.AEQU), where the regional mean $f\mathrm{CO_2}$ increases by 4.2 μatm from the year 2021 to 2022 (Figure S6). However, such a high increment in the AEQU $f\mathrm{CO_2}$ is negligible in terms of its contribution to the global net ocean sink variations between the two years (Figure S8 and Table S5). In Rödenbeck et al. (2015) [Figures A2 and A4], it is also illustrated that $p\mathrm{CO_2}^{\mathrm{sea}}$ ranges from 350 μatm to 400 μatm over an 18-year period while the AEQU net flux has performed with nearly constant magnitude. Its low interannual variability is in contrast with the eastern equatorial Pacific (9.PEQU-E) showing the strong impact on temporal variations of the global net sink (Figure S8). The signature of $f\mathrm{CO_2}$ dampening (-9.4 μatm) over PEQU-E in Jan to August of 2022-2023 is opposed to its increasing (1.8 μatm) with respect to 2021-2022 (Figure S6). As illustrated in Figures S8 and S9, FFNNv2022 prediction marks an anomalous decline of CO_2 source in the first eight months of 2023 (-0.30 ± 0.04 PgC.yr^{-1}) compared to that of 2022 (-0.37 ± 0.04 PgC.yr^{-1}). This reduced source of 0.07 PgC.yr^{-1} in PEQU-E contributes to 25% of the increase in the global ocean sink mentioned above. The reduction in the PEQU-E CO_2 source marks the transition from La Niña to El Niño announced by e.g., WMO (`https://public.wmo.int/en/media/press-release/world-meteorological-organization-declares-onset-of-el-ni%C3%B1o-conditions`, last access: 05/9/2023).

While the onset of El Niño over the tropical Pacific (Figure S9a) had been driving the reduction of ocean CO_2 emission La Niña anomalies (Figure S8), an exceptional warming event occurred and spread over the north Atlantic since May-June 2023 (Copernicus Climate Change Service: `https://climate.copernicus.eu/copernicus-record-north`

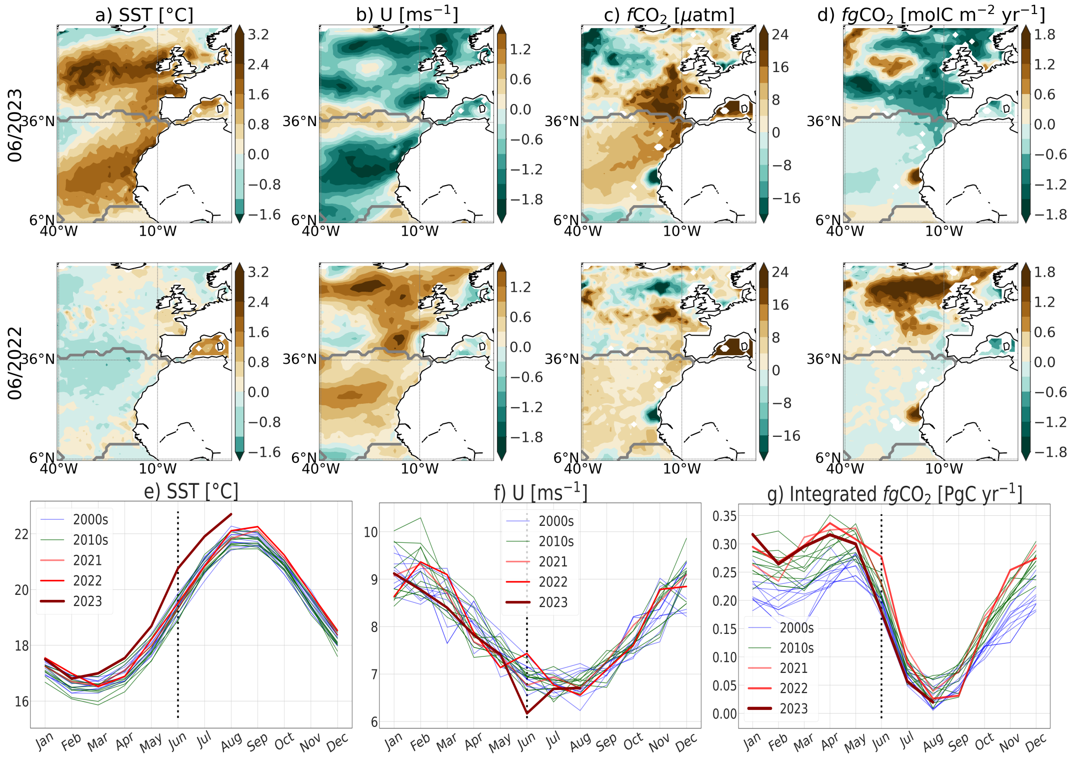

Figure 3. Top panels (a-d): anomalies observed in FFNNv2022 prediction of fCO_2 and $fgCO_2$ (c,d) follow an extreme marine heatwave event (a,b) over the northeastern Atlantic in June 2023 relative to June 2022 (top panels). Anomalies of surface temperature (SST), wind speed (U), fCO_2, and $fgCO_2$ are computed by subtracting long-term trends and seasonal climatologies relative to the years 1985-2022. Grey curve represents regional division (Figure S1). Bottom panels (e-g): regional seasonal cycles of SST, U, and integrated air-sea fluxes since 2000s.

`-atlantic-warmth-hottest-june-record-globally`, last access: 20/9/2023). It substantially lessened the ocean CO_2 uptake (Figure 3). Based on the CMEMS SST analyses (Table S1), June 2023 corresponds to the first marine extreme heatwave in the northeastern Atlantic (40°W-12°E, 5°N-65°N) with an average SST anomaly about 1.1°C (Figure 3ae). As a comparison, the June anomaly had been typically in a range of -0.5°C to 0.5°C for the past three decades. In 2023, SST anomalies even exceeded 1.5°C over the northeastern Atlantic seasonally stratified biome (NA-SS, 36°N northward). FFNNv2022 predicts an enhancement in fCO_2 (Figure 3c) following the anomalous warmth in the northeastern Atlantic which is not seen in June 2022 (Figure 3a). As other environmental factors (e.g., salinity and chlorophyll-a) have no remarkable anomalies over this ocean basin (Figure S10), warming primarily reduces CO_2 solubility and that leads to substantially high surface partial pressure of CO_2 (Figure 3c). fCO_2 anomalies were mostly between 4 μatm and 12 μatm in the subtropics, i.e., north Altlantic permanently stratified region (NA-PS) and increased eastward. FFNNv2022 records the largest fCO_2 anomalies in the southeast of NA-SS towards the European coast with values above 16 μatm. Consequently, the predicted air-sea fluxes in June 2023 (Figure 3d) suggest lower-than-average CO_2 uptake capability. While $fgCO_2$ slightly decreased throughout the NA-PS, an anomalous drawdown is found in the NA-SS exceeding -0.6 molC.m^{-2}.yr^{-1} (equivalent to roughly a reduction in ocean CO_2 uptake of 0.11 PgC.yr^{-1}). It is noteworthy that a decline in ocean CO_2 uptake is strengthened if surface wind speeds (U) are lowering and fCO_2 increases. Accompanied by the largest positive SST anomaly in June 2023, there is an unusual reduction in wind intensity, i.e., U anomalies potentially below -1.2 m.s^{-1} as illustrated in Figure 3b. Overall, regional seasonal cycles plotted for each year show the 2023 SST mostly on top of those in the past (Figure 3e). The most striking warmth recorded in June 2023 was at 1.24°C above that in June 2022. July and August 2023 followed up with SST increasing but the SST values are less different from 2022 then (1.06°C and 0.59°C respectively). Also in June 2023, wind speed dropped out of the lower bound of all seasonal cycles and the difference from the previous year was about -1.26 m.s^{-1} (Figure 3f). The combined anomalies in June 2023 marine extreme heat waves set the northeastern Atlantic ocean sink from an enhanced sink in 2022 (0.29 PgC.yr^{-1}) back to its magnitude in the 2000s (0.18 PgC yr^{-1}) (Figure 3g).

4 Conclusions and Perspectives

This study first examined the skill of CMEMS-LSCE-FFNN, an ensemble approach of feed-forward neural networks (FFNN) developed by Chau et al. (2022b), in a retrospective prediction of CO_2 fugacity (fCO_2) over the global ocean. The assessment was done for two FFNN models. While the latest version (FFNNv2022) trained on SOCATv2022 data for the period 1985-2021 was used to predict fCO_2 in 2022, FFNNv2021 trained on SOCATv2021 in 1985-2020 was used to predict fCO_2 in 2021-2022 allowing the qualification of the two-year model prediction. SOCATv2023 with data available in the prediction years was used for the prediction assessment. Our evaluation confirms a robust performance of the FFNN prediction in comparison to independent observation-based data and to the FFNN reconstruction. The retrospective prediction for the years 2021-2022 retained intra-seasonal to interannual variations of fCO_2 as those in the reconstruction time series and no large systematic bias has been observed between the two across all ocean provinces. The closeness between the predicted and reconstructed global net ocean budget implies that, when used as input to an atmospheric transport model, the prediction removes an appropriate mass of carbon from the simulated atmosphere: this is an important asset for greenhouse gas monitoring.

The latest model version, FFNNv2022, was ultimately used to predict $f\text{CO}_2$ from January 2022 to August 2023, i.e., up to 20 months beyond the coverage of its training dataset. This study also exemplified the assessment of air-sea CO_2 fluxes ($fg\text{CO}_2$) generated from the predicted $f\text{CO}_2$ in the years 2022-2023 over the eastern tropical Pacific, where regional CO_2 gas exchanges greatly vary with El Niño-Southern Oscillation (ENSO) conditions and thus affect substantially on interannual variability of the global net sink. The year 2022 has been predicted with persistently high $f\text{CO}_2$ (strong CO_2 outgassing to the atmosphere) in response to the maintenance of La Niña since summer 2020. A remarkable reduction in the tropical Pacific CO_2 source in August 2023 relative to the year before coincides with the weakening of the cooling phase. Recent discussions about the interaction between the ocean and climate have largely put attention on the El Niño revisits, their high possibility in triggering more extreme heat worldwide, and further impacts on the marine carbon cycle early at the end of 2023 onwards. However, already in June 2023 as exceptional surface ocean warming and extraordinarily low wind intensity fall out historical records over the north-eastern Atlantic ocean, we have found an anomalous reduction in CO_2 uptake setting this regional sink back to its magnitude in the 2000s. These results emphasise critical needs and open the possibility to derive monthly predictions for global surface ocean maps of numerous variables driven by $f\text{CO}_2$, including air-sea fluxes, seawater pH, and dissolved inorganic carbon, as the reconstruction quality of $f\text{CO}_2$ drives that of the other variables (Chau et al., 2022a, 2022b). The new datasets for the year 2022 (January) to 2023 (August) are available via the LSCE/IPSL data center (see Section Data availability) and are updated each month. This demonstration of an operational service will be extended at an increased horizontal resolution, following the current development of the reference CMEMS-LSCE-FFNN reconstructions (Chau et al., 2023).

Data availability

Data provided in this research are available for use with open access granted by the French LSCE/IPSL Data Center (`https://dods.lsce.ipsl.fr/invsat/FFNN_low-latency/`).

Acknowledgments

We acknowledge funding support by the MOB TAC project of the European Copernicus Marine Environment Monitoring Service (CMEMS, `https://marine.copernicus.eu/about/producers/mob-tac`, last access: 20/9/2023). SOCAT is an international effort endorsed by the International Ocean Carbon Coordination Project (IOCCP), the Surface Ocean Lower Atmosphere Study (SOLAS) and the Integrated Marine Biogeochemistry and Ecosystem Research program (IMBER), to deliver a uniformly quality-controlled surface ocean CO_2 database. The data center LSCE/IPSL has offered data repository and access. We thank François-Marie Bréon for the tool development of $x\mathrm{CO}_2$ extrapolation and comments on the first manuscript version and we thank Cédric Bacour for his help in running the extrapolation tool.

References

Bakker, D., Alin, S., Becker, M., Bittig, H., Castaño-Primo, R., Feely, R. A., ... others (2022). *Socat version 2022 for quantification of ocean co$_2$ uptake.* Retrieved from `https://socat.info/index.php/version-2022/` doi: https://doi.org/10.25921/1h9f-nb73

Bakker, D., Alin, S., Castaño-Primo, R., Margot, C., Gritzalis, T., Kozyr, A., ... others (2021). *Socat version 2021 for quantification of ocean co$_2$ uptake.* Retrieved from `https://socat.info/index.php/version-2021/`

Bakker, D., Alin, S. R., Bates, N., Becker, M., Feely, R. A., Gkritzalis, T., ... others (2023). *Surface ocean co$_2$ atlas database version 2023 (socatv2023).* doi: https://doi.org/10.25921/r7xa-bt92

Bakker, D., Pfeil, B., Landa, C. S., Metzl, N., O'Brien, K. M., Olsen, A., ... Xu, S. (2016). A multi-decade record of high-quality $f\mathrm{co}_2$ data in version 3 of the surface ocean co$_2$ atlas (socat). *Earth System Science Data*, *8*(2), 383–413. Retrieved from `https://essd.copernicus.org/articles/8/383/2016/` doi: 10.5194/essd-8-383-2016

Bates, N. R., Astor, Y. M., Church, M. J., Currie, K., Dore, J. E., González-Dávila, M., ... Santana-Casiano, J. M. (2014). A time-series view of changing surface ocean chemistry due to ocean uptake of anthropogenic co$_2$ and ocean acidification. *Oceanography*, *27*(1), 126–141.

Canadell, J. G., Monteiro, P. M., Costa, M. H., Da Cunha, L. C., Cox, P. M., Alexey, V., ... others (2021). Global carbon and other biogeochemical cycles and feedbacks in climate change 2021: The physical science basis. contribution of working group i to the sixth assessment report of the intergovernmental panel on climate change. Cambridge University Press. doi: 10.1017/9781009157896.007

Chau, T. T. T., Gehlen, M., & Chevallier, F. (2022a, December). *Global ocean surface carbon product* (Research Report No. CMEMS-MOB-QUID-015-008). Le Laboratoire des Sciences du Climat et de l'Environnement. Retrieved from `https://hal.archives-ouvertes.fr/hal-02957656` (Quality Information Document) doi: 10.48670/moi-00047

Chau, T. T. T., Gehlen, M., & Chevallier, F. (2022b). A seamless ensemble-based reconstruction of surface ocean $p\text{co}_2$ and air–sea co_2 fluxes over the global coastal and open oceans. *Biogeosciences*, *19*(4), 1087–1109. Retrieved from `https://bg.copernicus.org/articles/19/1087/2022/` doi: 10.5194/bg-19-1087-2022

Chau, T. T. T., Gehlen, M., Metzl, N., & Chevallier, F. (2023). Cmems-lsce: A global 0.25-degree, monthly reconstruction of the surface ocean carbonate system. *Earth System Science Data Discussions*, *2023*, 1–52. doi: 10.5194/essd-2023-146

Cooley, S., Schoeman, D., Bopp, L., Boyd, P., Donner, S., Ito, S.-i., ... others (2022). Oceans and coastal ecosystems and their services. In *Ipcc ar6 wgii*. Cambridge University Press.

Doney, S. C., Busch, D. S., Cooley, S. R., & Kroeker, K. J. (2020). The impacts of ocean acidification on marine ecosystems and reliant human communities. *Annual Review of Environment and Resources*, *45*(1).

Fay, A. R., & McKinley, G. A. (2014). Global open-ocean biomes: mean and temporal variability. *Earth System Science Data*, *6*(2), 273–284. Retrieved from `https://essd.copernicus.org/articles/6/273/2014/` doi: 10.5194/essd-6-273-2014

Friedlingstein, P., O'Sullivan, M., Jones, M. W., Andrew, R. M., Gregor, L., Hauck, J., ... Zheng, B. (2022). Global carbon budget 2022. *Earth System Science Data*, *14*(11), 4811–4900. Retrieved from `https://essd.copernicus.org/articles/14/4811/2022/` doi: 10.5194/essd-14-4811-2022

Gallego, M., Timmermann, A., Friedrich, T., & Zeebe, R. E. (2018). Drivers of future seasonal cycle changes in oceanic pco 2. *Biogeosciences*, *15*(17), 5315–5327.

Gregor, L., & Gruber, N. (2021). Oceansoda-ethz: a global gridded data set of the surface ocean carbonate system for seasonal to decadal studies of ocean acidification. *Earth System Science Data*, *13*(2), 777–808. Retrieved from `https://essd.copernicus`

.org/articles/13/777/2021/ doi: 10.5194/essd-13-777-2021

Gregor, L., Lebehot, A. D., Kok, S., & Scheel Monteiro, P. M. (2019). A comparative assessment of the uncertainties of global surface ocean CO_2 estimates using a machine-learning ensemble (csir-ml6 version 2019a) – have we hit the wall? *Geoscientific Model Development*, *12*(12), 5113–5136. Retrieved from https://gmd.copernicus.org/articles/12/5113/2019/ doi: 10.5194/gmd-12-5113-2019

Gruber, N., Bakker, D. C., DeVries, T., Gregor, L., Hauck, J., Landschützer, P., ... Müller, J. D. (2023). Trends and variability in the ocean carbon sink. *Nature Reviews Earth & Environment*, *4*(2), 119–134.

Gruber, N., Landschützer, P., & Lovenduski, N. S. (2019). The variable southern ocean carbon sink. *Annual review of marine science*, *11*, 159–186.

Hopkins, F. E., Suntharalingam, P., Gehlen, M., Andrews, O., Archer, S. D., Bopp, L., ... others (2020). The impacts of ocean acidification on marine trace gases and the implications for atmospheric chemistry and climate. *Proceedings of the Royal Society A*, *476*(2237), 20190769.

Janssens-Maenhout, G., Pinty, B., Dowell, M., Zunker, H., Andersson, E., Balsamo, G., ... others (2020). Toward an operational anthropogenic co 2 emissions monitoring and verification support capacity. *Bulletin of the American Meteorological Society*, *101*(8), E1439–E1451.

Landschützer, P., Gruber, N., & Bakker, D. C. (2016). Decadal variations and trends of the global ocean carbon sink. *Global Biogeochemical Cycles*, *30*(10), 1396–1417.

Landschützer, P., Ilyina, T., & Lovenduski, N. S. (2019). Detecting regional modes of variability in observation-based surface ocean pco_2. *Geophysical Research Letters*, *46*(5), 2670–2679.

Regnier, P., Resplandy, L., Najjar, R. G., & Ciais, P. (2022). The land-to-ocean loops of the global carbon cycle. *Nature*, *603*(7901), 401–410.

Rödenbeck, C., Bakker, D. C. E., Gruber, N., Iida, Y., Jacobson, A. R., Jones, S., ... Zeng, J. (2015). Data-based estimates of the ocean carbon sink variability – first results of the surface ocean pco_2 mapping intercomparison (socom). *Biogeosciences*, *12*(23), 7251–7278. Retrieved from https://bg.copernicus.org/articles/12/7251/2015/ doi: 10.5194/bg-12-7251-2015

Rödenbeck, C., Keeling, R. F., Bakker, D. C., Metzl, N., Olsen, A., Sabine, C., & Heimann, M. (2013). Global surface-ocean pco_2 and sea–air co_2 flux variability from an observation-driven ocean mixed-layer scheme. *Ocean Science*, *9*(2), 193–216.

Rustogi, P., Landschützer, P., Brune, S., & Baehr, J. (2023). The impact of seasonality on the annual air-sea carbon flux and its interannual variability. *npj Climate and Atmospheric Science*, *6*(1), 66.

Takahashi, T., Sutherland, S. C., Sweeney, C., Poisson, A., Metzl, N., Tilbrook, B., … others (2002). Global sea–air co2 flux based on climatological surface ocean pco2, and seasonal biological and temperature effects. *Deep Sea Research Part II: Topical Studies in Oceanography*, *49*(9-10), 1601–1622.

Global analysis of surface ocean CO_2 fugacity and air-sea fluxes with low latency

Thi-Tuyet-Trang Chau[1], **Frédéric Chevallier**[1], **and Marion Gehlen**[1]

[1]Laboratoire des Sciences du Climat et de l'Environnement, LSCE/IPSL, CEA-CNRS-UVSQ, Université Paris-Saclay, F-91191 Gif-sur-Yvette, France

Key Points:

- We demonstrate the capacity of statistical models to generate global maps of $f\mathrm{CO}_2$ and air-sea flux with a latency reduced to one month.
- A decrease in the CO_2 source for January to August 2023 diagnosed in the tropical Pacific coheres with the retreat of the La Niña event.
- An unusual northeastern Atlantic sink reduction diagnosed for June 2023 is linked to record heat and exceptionally low winds.

Corresponding author: Thi-Tuyet-Trang Chau, `thi.tuyet.trang.chau@gmail.com`

Abstract

The Surface Ocean CO_2 Atlas (SOCAT) of CO_2 fugacity ($f CO_2$) observations is a key resource supporting annual assessments of CO_2 uptake by the ocean and its side effects on the marine ecosystem. SOCAT data are usually released with a lag of up to 1.5 years which hampers timely quantification of recent variations of carbon fluxes between the Earth System components, not only with the ocean. This study uses a statistical ensemble approach to analyse $f CO_2$ with a latency of one month only based on the previous SOCAT release and a series of predictors. A retrospective prediction for the years 2021-2022 is made to test the model skill, followed by the generation of $f CO_2$ and fluxes from January to August in 2023. Results indicate a modest degradation of the model skill in prediction mode and open the possibility to provide robust information about marine carbonate system variables with low latency.

Plain Language Summary

There is a growing need to monitor carbon emissions and removals over the globe in near real time in order to correctly interpret changes in CO_2 concentrations as they unfold. For the oceans, the best information comes from measurements of the surface ocean CO_2 fugacity ($f CO_2$) by the international marine carbon research community. So far, this data is mostly available 6 to 18 months behind real time after collection, qualification, harmonization, and processing. Here, we show that a set of biological, chemical, and physical predictors available in near-real time, allows the information contained in the "old" $f CO_2$ measurements to be transferred over time. Based on a statistical technique, we combine all these data sources to estimate global monthly maps of $f CO_2$ and of CO_2 fluxes at the air-sea interface within one month behind real time and with good accuracy.

1 Introduction

The ocean is a sink taking up about 26% of atmospheric carbon dioxide (CO_2) and 90% of the heat-induced largely by anthropogenic greenhouse gas emissions (Canadell et al., 2021; Friedlingstein et al., 2022). A side effect of the ocean's role as a global climate modulator is the increase in seawater acidity, which dramatically affects marine ecosystems (Hopkins et al., 2020; Doney et al., 2020; Cooley et al., 2022). The global ocean carbon sink is proportional to CO_2 human emissions only at the decadal scale. On shorter time scales, it varies with the climate (mostly temperature and winds), with a dependency that also varies from basin to basin given their respective geographical, dynamic, and biological specificities (Rödenbeck et al., 2015; Landschützer et al., 2016; Gruber et al., 2023).

Measurements of surface ocean CO_2 fugacity (fCO_2) from ships, drifters, moorings, and autonomous surface platforms are the main reference to document the actual variation of air-sea fluxes ($fgCO_2$) in space and time (Friedlingstein et al., 2022) because the two are linearly related. Long-term efforts in maintaining and expanding international observing networks together with a coordinated data aggregation of the Surface Ocean CO_2 Atlas database - SOCAT (Bakker et al., 2016, 2023) have provided millions of individual fCO_2 observations since the 1950s and associated gridded products. However, fCO_2 data are poorly sampled leaving out most areas for some or all of the year. Statistical data-based reconstructions of fCO_2 (Rödenbeck et al., 2013; Landschützer et al., 2016; Gregor & Gruber, 2021; Chau et al., 2022b) have emerged to gap-fill the SOCAT database using auxiliary data, resulting in reconstructions of fCO_2 global monthly maps. They are still the topic of active research to improve the reconstruction quality, but these maps lag behind real time by 0.5 to 1.5 years: the update of the SOCAT archive follows an annual pace with a public release usually in June after measurement collection, quality control, and processing. This lag is problematic for the documentation of the carbon cycle as it evolves, while the main variables of the carbon cycle are progressively integrated within operational programmes with much faster data releases. A prominent example of operational programmes in need of a reduced time lag is the operational observation-based anthropogenic CO_2 emissions monitoring and verification support capacity (CO_2MVS) that the European Commission is building under its Copernicus Earth Observation programme (e.g., Janssens-Maenhout et al. (2020)). As its observational component relies heavily on satellite observations of CO_2 in the atmosphere, which is affected by the ocean as well as terrestrial emissions and removals, better estimates of fCO_2 would result in efficient estimates of air-sea fluxes and thence benefit air-land flux accuracy, in addition to being directly interesting to users. The CO_2MVS fits within the Global Greenhouse Gas Watch, an even larger greenhouse gas monitoring infrastructure that the World Meteorological Organization (WMO) is setting up (`https://public.wmo.int/en/media/press-release/world-meteorological-congress-approves-global-greenhouse-gas-watch`, last access: 20/9/2023).

Here, we demonstrate the capability to retrieve global monthly maps of fCO_2 from SOCAT data and then to generate the corresponding fields of air-sea fluxes with a lag reduced to one month. To do that, we extend the work of Chau et al. (2022b) who have been gap-filling SOCAT gridded data within the framework of the Copernicus Marine Environment Monitoring Service (CMEMS) based on an ensemble of feed-forward neural network models (also referred to as CMEMS-LSCE-FFNN) and a set of biological, chemical, and physical predictors. While Chau et al. (2022b) made the dates of the predictors and the date of the gridded SOCAT data coincide, we turn to a prediction mode in which the relationship found between the predictors and the SOCAT data more than 6 months before is kept. Section 2 below describes the method. We test the approach in the years 2021-2022 by examining the retrospective prediction skill based on the available SOCAT data. Then we expand model prediction of $f\mathrm{CO_2}$ and generate $fg\mathrm{CO_2}$ up to present with a latency of 1 month: data access via the Institut Pierre-Simon Laplace (LSCE/IPSL) data center, `https://dods.lsce.ipsl.fr/invsat/FFNN_low-latency/`. The results include the finding of anomalous variations in regional $\mathrm{CO_2}$ uptake and release by the ocean predicted in January to August 2023, as described in Section 3. Section 4 draws the main conclusions of the study.

2 Materials and Methods

CMEMS-LSCE-FFNN (Chau et al., 2022b) is built on machine-learning techniques. It consists of an ensemble of feed-forward neural network (FFNN) models. This ensemble approach was developed at LSCE in order to reconstruct surface ocean carbonate system variables and to support the operational distribution of such datasets by CMEMS since 2019 (Product identity: MULTIOBS_GLO_BIO_CARBON_SURFACE_REP_015_008, `https://doi.org/10.48670/moi-00047`, last access: 22/9/2023). The CMEMS-LSCE-FFNN fields cover the global ocean at a resolution of $1^\circ \times 1^\circ$ currently and for the period since the year 1985 at monthly resolution.

Under the hood, these FFNN models represent nonlinear mappings of $f\mathrm{CO_2}$ against a set of predictors. Monthly gridded observation-based products of $f\mathrm{CO_2}$ from SOCAT (Bakker et al., 2016) are used as the target data in model fitting. $f\mathrm{CO_2}$ predictors are environmental variables: sea surface temperature (SST), sea surface salinity (SSS), sea surface height (SSH), chlorophyll-a (Chl-a), mix-layer-depth (MLD), $\mathrm{CO_2}$ surface mole fractions ($x\mathrm{CO_2}$), climatological $f\mathrm{CO_2}$ ($f\mathrm{CO_2}^{\mathrm{clim}}$), and geographical coordinates (latitude and longitude). Product resources of input datasets are detailed in Table S1. CMEMS-LSCE-FFNN comprises monthly adaptive FFNN models for which the $f\mathrm{CO_2}$ and predictor datasets available within a time span of 3 months for all the years since 1985 (the reconstruction month excepted) are used in the fitting phase. SOCAT $f\mathrm{CO_2}$ in the reconstruction month is only used in model evaluation. The ensemble of multi-FFNN models was designed by randomly splitting two-thirds of the 3-month sliding datasets for training and the rest for model test (Chau et al., 2022b). From the ensemble reconstructions, the model best estimate (ensemble mean) and 1σ - model uncertainty (ensemble standard deviation) of $f\mathrm{CO_2}$ are derived at the desired resolution.

Here we revisit the two versions of CMEMS-LSCE-FFNN referred to as FFNNv2021 and FFNNv2022. These two models respectively used SOCATv2021 and SOCATv2022 datasets (Bakker et al., 2021, 2022) as the target input data of $f\mathrm{CO_2}$. Note that SOCAT has been annually published mid-June. Due to the delay mode for data collection, reprocessing, and qualify control, SOCAT provides gridded data up to the year before the publication date (see Bakker et al. (2016, 2023) for instance). For the period 1985-2021, SOCATv2022 offers an amount of roughly 311700 monthly 1-degree gridded data, 5000 more than SOCATv2021 (Table S3a). The data increase in SOCATv2022 is mostly distributed within the last three years due to the late availability of some data sources (Figure 1). However, SOCATv2021 has more data before 2018, up to at least 1000 more in some years (e.g., 2011 and 2012) due to an erroneous flagging of some data (Bakker et al., 2021). Despite this feature, the two corresponding FFNN reconstructions do not exhibit large systematic offsets in their $f\mathrm{CO_2}$ estimates (Chau et al., 2022a).

For all experiments in this study, the ensemble size (i.e., number of FFNN model runs) is set to 50. FFNN with 50 ensemble members has less computational complexity than with the usual size of 100 but it shows similar reconstruction skill (Chau et al. (2022b); Figure S2). The same input data of predictors is fed to the two FFNN model runs (Table S1). The FFNNv2021 (respectively FFNNv2022) model relies on SOCATv2021 (respectively SOCATv2022) and predictor datasets in 1985-2020 (respectively 1985-2021). This allows deriving the ensemble global reconstructions of $f\mathrm{CO_2}$ over the 36-year and 37-year periods, accordingly. The ensemble of FFNN models is then applied to predict $f\mathrm{CO_2}$ given the set of predictors in the years 2021-2022 for version 2021 and in the year 2022 for the latter. The quality assessments are made for (1) the two global reconstructions in the period 1985-2020, (2) FFNNv2021 one-year prediction against FFNNv2022 one-year reconstruction in 2021, and (3) FFNNv2021 two-year prediction against FFNNv2022 one-year prediction in 2022. Model performances will be qualified with the latest SOCAT data, i.e., SOCATv2023 (Bakker et al., 2023). The number of evaluation data for prediction in the years 2021 and

2022 over the global ocean is 10908 and 8602, respectively (Table S3a), which is statistically sufficient for significant validation.

Model skills are examined from global to sub-basin scale. Here we consider the sub-basins defined by the REgional Carbon Cycle Assessment and Processes2 project (`https://github.com/RECCAP2-ocean/RECCAP2-shared-resources/tree/master/data/regions`, last access: 20/3/2023). Due to a lack of evaluation data in several RECCAP2 biomes, we aggregate some of them, yielding 14 provinces in total (see Table S2 and Figure S1). These ocean provinces, therefore, differ from the original biomes proposed by Fay and McKinley (2014). Apart from the Northern Indian Ocean (11.NIO), the number of data for prediction evaluation ranges from 133 (12.SIO, i.e., Southern Indian Ocean) to 2350 (2.NA-SS, i.e., North Atlantic seasonally stratified) in the year 2021 and from 73 to 2265 in the year 2022.

For the actual prediction in 2022 and 2023, the latest model (FFNNv2022) has been run given monthly data of predictors (Table S1) in the year 2022 to present. We choose to release the maps of $f\mathrm{CO}_2$ and $fg\mathrm{CO}_2$ for the previous month on the 15th of each month.

3 Evaluation and Discussions

3.1 Reconstruction and Prediction of $\mathbf{CO_2}$ fugacity in 1985-2022

3.1.1 Global qualification

FFNNv2021 and FFNNv2022 share consistent global RMSD and determination coefficient r^2 (Figure 1 and Table S3). Between 1985 and 2020, the two reconstructions inherit the same RMSD of 19.1 μatm and r^2 of 0.78 (Table S3b). Improvement in the global reconstruction skill of FFNNv2022 in recent years (Figure 1b) is moderate despite 5000 additional $f\mathrm{CO}_2$ data in the model training (Figure 1a). In detail, these 1.7% additional data in SOCATv2022 (311694 in total) in 1985-2021 correspond to 9615 data added in 2021 and 4278 data removed from SOCATv2021 in 1985-2020 (see the spatial distribution of removal data in Figure S2c).

The RMSD variability before 2018 (Figure 1b) is likely linked to changes in the data sampling in regions with high spatiotemporal variability of $f\mathrm{CO}_2$ (see Gregor et al. (2019); Chau et al. (2022b) for further analysis). However, the difference between the RMSD of the two reconstructions is negligible then, as it fluctuates within $[-0.1, 0.1]$ μatm. During the last four years, a monotonous increase in RMSD (Figure 1b) coexists with a decrease in

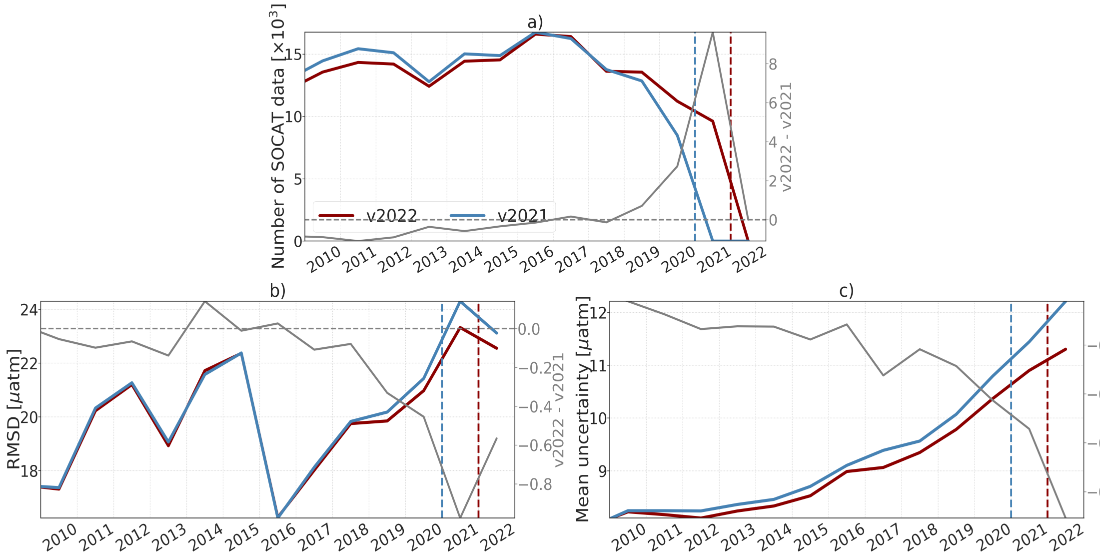

Figure 1. (a) Number of data per year in SOCATv2021 and SOCATv2022, (b) RMSD of FFNNv2021 and FFNNv2022 against SOCATv2023 fCO_2, (c) yearly global mean uncertainty (1σ). Differences between the two versions are shown with a grey solid curve with values on the right y-axis whereas the grey solid curve below 0 (grey dashed horizontal line). The blue and red vertical lines mark the start of the prediction mode for FFNNv2021 and FFNNv2022, respectively.

the number of SOCAT data (Figure 1a), and the FFNNv2021 reconstruction slightly, but increasingly, underperforms compared to FFNNv2022. In 2021 and 2022, the FFNNv2021 prediction RMSD is 24.3 μatm and 23.1 μatm, respectively, roughly $0.5-1$ μatm higher than that of the FFNNv2022 reconstruction and prediction (Table S3). Likewise, the variation of SOCAT fCO_2 is reproduced with high r^2 values (0.74 and 0.75), close to the one-year reconstruction and prediction of FFNNv2022 (0.76) for the years 2021-2022.

The yearly-mean uncertainty over the global ocean (Figure 1c) is computed by weighting the model estimated uncertainty (ensemble spread) per grid cell (σ) with the geographical area. The two reconstructions before the year 2015 are rather stable with an uncertainty about 8.5 μatm. The increase in FFNNv2021 [v2022] model uncertainty from 8.7 μatm [8.5 μatm] to 10.8 μatm [10.4 μatm] between 2015-2020 follows a decrease in observation-based data from 14877 [14533] to 8482 [11217] (Figure 1a). In the year 2021, the FFNNv2021 uncertainty of predicted fCO_2 (11.4 μatm) is slightly higher than that of the FFNNv2022 reconstruction but the offset between the two values is as small as 0.5 μatm (Figure 1c). The prediction uncertainty in 2022 increases by $0.4 - 0.8$ μatm for the two models (FFNNv2021: 12.2 μatm, FFNNv2022: 11.3 μatm).

3.1.2 Regional assessment

Model reconstruction and prediction skills are assessed over 14 ocean provinces (Figure S1 and Table S2) in the years 1985-2020 and 2021-2022 (1985-2021 and 2022) for FFNNv2021 (FFNNv2022). Results of the regional evaluation are summarized in Figure 2 and Table S4. The two FFNN models perform with a similar skill in reconstruction mode (1985-2020) over all ocean provinces. Evidently, their reconstructions share consistent patterns in regional-mean fCO_2 (Figure 2b) and in the spatial and temporal variations (Figures S4abc and S7) with systematic biases below 1 μatm for most of the basins (Table S4). Differences in uncertainty estimates and RMSD do not exceed 0.5 μatm while those in r^2 are nearly the same (Figure 2cde and Table S4).

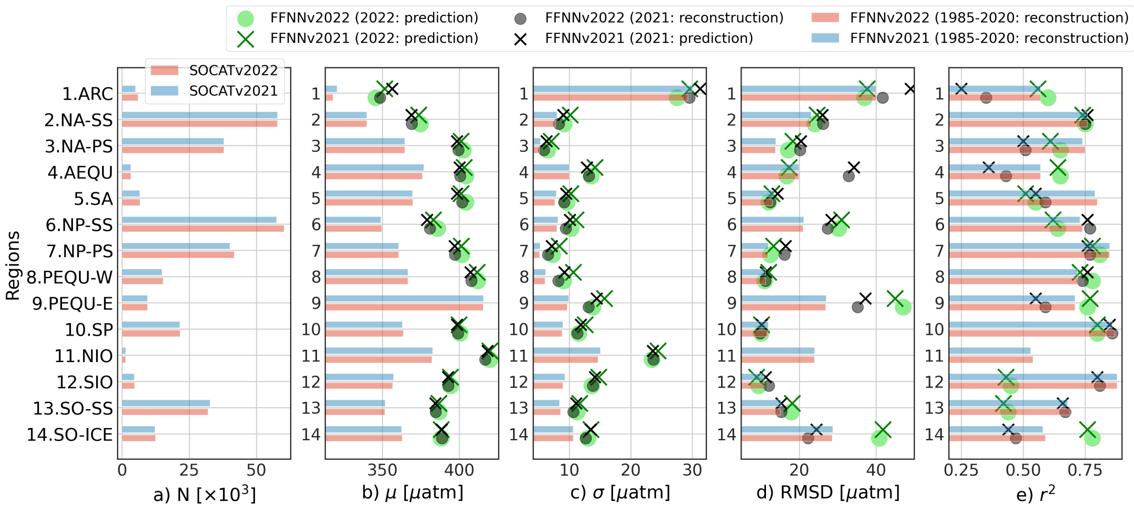

Figure 2. Regional comparisons of the two FFNN reconstructions in 1985-2020 (bars) and of the FFNNv2021 prediction versus the FFNNv2022 reconstruction [prediction] in 2021 [2022] (objects) in terms of (a) N- number of SOCAT monthly gridded data used in model fitting, (b) μ- mean fCO_2, (c) σ-mean uncertainty, (d) RMSD model-data deviation, and (e) r^2 model-data correlation.

In the years 2021-2022, RMSD (r^2) of the FFNN prediction does not change from the full-period reconstruction by more than about 5 μatm (0.1) over many sub-basins (e.g., 2.NA-SS, 7.NP-PS, 8.PEQU-W, 10.SP, 12.SIO, and 13.SO-SS). As expected, FFNNv2022 (one-year prediction) performs slightly better than FFNNv2021 (two-year prediction) in the

2022 prediction for many regions (Figures 2de and Table S4). However, the differences in regional skill scores of the two models are substantially small, i.e., below 3 μatm for RMSD and 0.05 for r^2. These results suggest a high confidence level in FFNN prediction for a few years ahead. The analysis of the spatial distribution and of the time series (Figures 2, S4, and S7) also reveals consistent features (horizontal gradients of $f\mathrm{CO_2}$ and seasonality to long-term variations) from the reconstruction years to the prediction years. $f\mathrm{CO_2}$ increases over time (see f.i., 7.NP-PS, 8.PEQU-W, 12.SIO) following the trend in atmospheric $\mathrm{CO_2}$ concentration. Among the $f\mathrm{CO_2}$ predictors, $x\mathrm{CO_2}$ stands out with its large increasing trend that brings some $x\mathrm{CO_2}$ data used in the prediction above the range of those used in the training. The growth of atmospheric $\mathrm{CO_2}$ is the primary factor driving the increase in sea surface $f\mathrm{CO_2}$ (Bates et al., 2014; Gruber et al., 2019; Landschützer et al., 2019; Friedlingstein et al., 2022). The prediction skill, however, does not degrade compared to the reconstruction as the annual increment of $f\mathrm{CO_2}$ is typically smaller than its intra-annual variability (Figure S6). The latter is dominantly driven by temperature-dependent $\mathrm{CO_2}$ solubility and biological processes (Takahashi et al., 2002; Gallego et al., 2018; Rustogi et al., 2023). The range of the pre-2021 [pre-2022] training datasets of physical and biological predictors (e.g., SST, Chl-a) remains similar to that including input data in the next year, seasonality to multi-month variations of $f\mathrm{CO_2}$ in the years 2021-2022 can be, therefore, propagated with these covariates overall. The majority of SOCAT $f\mathrm{CO_2}$ data for 2021 [2022] stays within the full range of training data which also supports FFNNs to achieve a skillful prediction (Figure S3). Further analysis of FFNN prediction skills over ocean basins is presented in the Supporting Information document.

3.2 Prediction of air-sea $\mathbf{CO_2}$ fluxes in 2022-2023

The previous results emphasize the skill and reliability of FFNN models in both reconstruction and prediction of $\mathrm{CO_2}$ fugacity ($f\mathrm{CO_2}$). In this section, we will use the FFNNv2022 predicted $f\mathrm{CO_2}$ field to generate corresponding air-sea fluxes ($fg\mathrm{CO_2}$) and analyze preliminary results for 20 months, from January 2022 to August 2023. $fg\mathrm{CO_2}$ is given in $\mathrm{molC.m^{-2}.yr^{-1}}$ for a flux density and in $\mathrm{PgC.yr^{-1}}$ for integration over ocean basins (see Supporting Information for details of flux calculation and analysis). FFNNv2022 predicts a reduction in the global ocean uptake of $\mathrm{CO_2}$ for 2022 (2.25 ± 0.5 $\mathrm{PgC.yr^{-1}}$) compared to the previous year (2.36 ± 0.43 $\mathrm{PgC.yr^{-1}}$). When adjusting the estimated global net fluxes with the riverine outgassing of $\mathrm{CO_2}$ of 0.65 $\mathrm{PgC.yr^{-1}}$ (Regnier et al., 2022) and the total ocean surface area (FFNNv2022 data covers 95% of the global ocean), one obtains the estimates of anthropogenic ocean carbon uptake consistent with the 2022 projection proposed by Friedlingstein et al. (2022): the anthropogenic ocean sink in 2021 was 2.9 ± 0.4 PgC.yr^{-1} remains unchanged for the year 2022. This evidence supports their hypothesis that the persistence of cooling climate patterns (La Niña conditions) weakened CO_2 ocean uptake in 2021-2022 (high peaks appeared mid-2022, Figure S9). FFNNv2022 predicts a global net flux of 2.45 ± 0.56 PgC.yr^{-1} for January to August 2023, the enhancement of global ocean uptake compared to that in 2022 (2.17 ± 0.50 PgC.yr^{-1}) is synchronous with the retreat of La Niña.

The model prediction retains the seasonal to interannual variations of $f\mathrm{CO_2}$ and $fg\mathrm{CO_2}$ in the pre-2022 reconstruction over many ocean basins (Figures S6 and S8). One of the remarkable changes is observed at the equatorial Atlantic (4.AEQU), where the regional mean $f\mathrm{CO_2}$ increases by 4.2 μatm from the year 2021 to 2022 (Figure S6). However, such a high increment in the AEQU $f\mathrm{CO_2}$ is negligible in terms of its contribution to the global net ocean sink variations between the two years (Figure S8 and Table S5). In Rödenbeck et al. (2015) [Figures A2 and A4], it is also illustrated that $p\mathrm{CO_2}^{\mathrm{sea}}$ ranges from 350 μatm to 400 μatm over an 18-year period while the AEQU net flux has performed with nearly constant magnitude. Its low interannual variability is in contrast with the eastern equatorial Pacific (9.PEQU-E) showing the strong impact on temporal variations of the global net sink (Figure S8). The signature of $f\mathrm{CO_2}$ dampening (-9.4 μatm) over PEQU-E in Jan to August of 2022-2023 is opposed to its increasing (1.8 μatm) with respect to 2021-2022 (Figure S6). As illustrated in Figures S8 and S9, FFNNv2022 prediction marks an anomalous decline of CO_2 source in the first eight months of 2023 (-0.30 ± 0.04 PgC.yr^{-1}) compared to that of 2022 (-0.37 ± 0.04 PgC.yr^{-1}). This reduced source of 0.07 PgC.yr^{-1} in PEQU-E contributes to 25% of the increase in the global ocean sink mentioned above. The reduction in the PEQU-E CO_2 source marks the transition from La Niña to El Niño announced by e.g., WMO (`https://public.wmo.int/en/media/press-release/world-meteorological-organization-declares-onset-of-el-ni%C3%B1o-conditions`, last access: 05/9/2023).

While the onset of El Niño over the tropical Pacific (Figure S9a) had been driving the reduction of ocean CO_2 emission La Niña anomalies (Figure S8), an exceptional warming event occurred and spread over the north Atlantic since May-June 2023 (Copernicus Climate Change Service: `https://climate.copernicus.eu/copernicus-record-north`

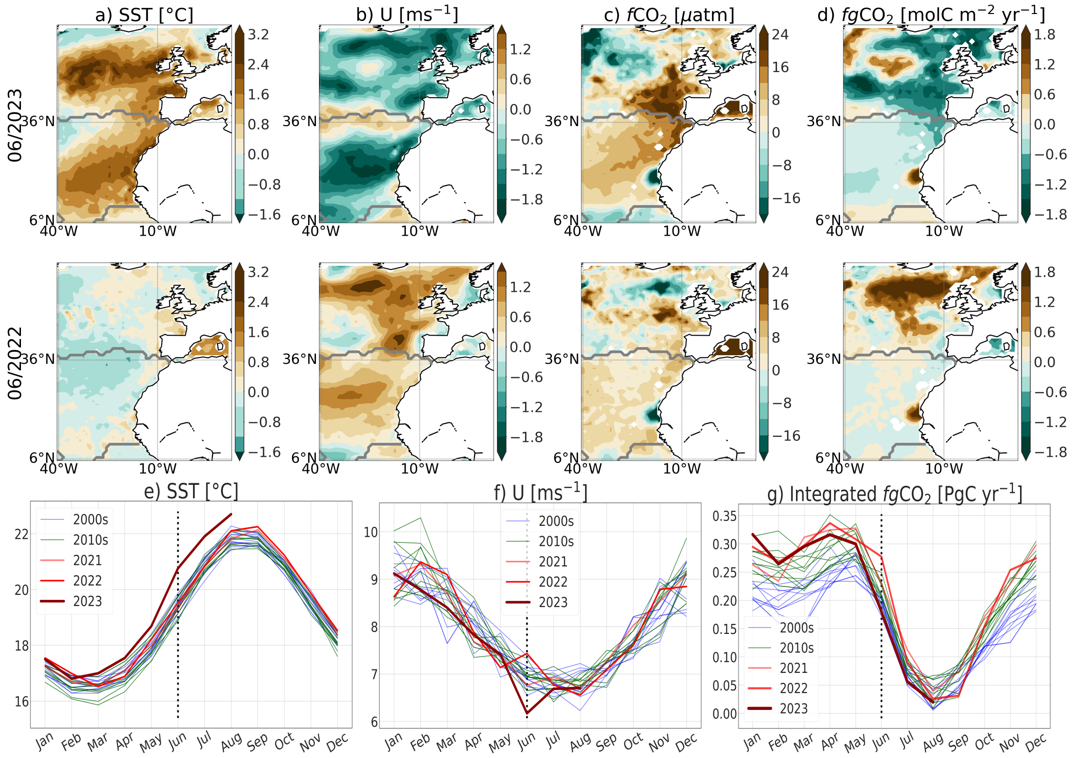

Figure 3. Top panels (a-d): anomalies observed in FFNNv2022 prediction of fCO_2 and $fgCO_2$ (c,d) follow an extreme marine heatwave event (a,b) over the northeastern Atlantic in June 2023 relative to June 2022 (top panels). Anomalies of surface temperature (SST), wind speed (U), fCO_2, and $fgCO_2$ are computed by subtracting long-term trends and seasonal climatologies relative to the years 1985-2022. Grey curve represents regional division (Figure S1). Bottom panels (e-g): regional seasonal cycles of SST, U, and integrated air-sea fluxes since 2000s.

`-atlantic-warmth-hottest-june-record-globally`, last access: 20/9/2023). It substantially lessened the ocean CO_2 uptake (Figure 3). Based on the CMEMS SST analyses (Table S1), June 2023 corresponds to the first marine extreme heatwave in the northeastern Atlantic (40°W-12°E, 5°N-65°N) with an average SST anomaly about 1.1°C (Figure 3ae). As a comparison, the June anomaly had been typically in a range of -0.5°C to 0.5°C for the past three decades. In 2023, SST anomalies even exceeded 1.5°C over the northeastern Atlantic seasonally stratified biome (NA-SS, 36°N northward). FFNNv2022 predicts an enhancement in fCO_2 (Figure 3c) following the anomalous warmth in the northeastern Atlantic which is not seen in June 2022 (Figure 3a). As other environmental factors (e.g., salinity and chlorophyll-a) have no remarkable anomalies over this ocean basin (Figure S10), warming primarily reduces CO_2 solubility and that leads to substantially high surface partial pressure of CO_2 (Figure 3c). fCO_2 anomalies were mostly between 4 μatm and 12 μatm in the subtropics, i.e., north Altlantic permanently stratified region (NA-PS) and increased eastward. FFNNv2022 records the largest fCO_2 anomalies in the southeast of NA-SS towards the European coast with values above 16 μatm. Consequently, the predicted air-sea fluxes in June 2023 (Figure 3d) suggest lower-than-average CO_2 uptake capability. While $fgCO_2$ slightly decreased throughout the NA-PS, an anomalous drawdown is found in the NA-SS exceeding -0.6 molC.m^{-2}.yr^{-1} (equivalent to roughly a reduction in ocean CO_2 uptake of 0.11 PgC.yr^{-1}). It is noteworthy that a decline in ocean CO_2 uptake is strengthened if surface wind speeds (U) are lowering and fCO_2 increases. Accompanied by the largest positive SST anomaly in June 2023, there is an unusual reduction in wind intensity, i.e., U anomalies potentially below -1.2 m.s^{-1} as illustrated in Figure 3b. Overall, regional seasonal cycles plotted for each year show the 2023 SST mostly on top of those in the past (Figure 3e). The most striking warmth recorded in June 2023 was at 1.24°C above that in June 2022. July and August 2023 followed up with SST increasing but the SST values are less different from 2022 then (1.06°C and 0.59°C respectively). Also in June 2023, wind speed dropped out of the lower bound of all seasonal cycles and the difference from the previous year was about -1.26 m.s^{-1} (Figure 3f). The combined anomalies in June 2023 marine extreme heat waves set the northeastern Atlantic ocean sink from an enhanced sink in 2022 (0.29 PgC.yr^{-1}) back to its magnitude in the 2000s (0.18 PgC yr^{-1}) (Figure 3g).

4 Conclusions and Perspectives

This study first examined the skill of CMEMS-LSCE-FFNN, an ensemble approach of feed-forward neural networks (FFNN) developed by Chau et al. (2022b), in a retrospective prediction of CO_2 fugacity (fCO_2) over the global ocean. The assessment was done for two FFNN models. While the latest version (FFNNv2022) trained on SOCATv2022 data for the period 1985-2021 was used to predict fCO_2 in 2022, FFNNv2021 trained on SOCATv2021 in 1985-2020 was used to predict fCO_2 in 2021-2022 allowing the qualification of the two-year model prediction. SOCATv2023 with data available in the prediction years was used for the prediction assessment. Our evaluation confirms a robust performance of the FFNN prediction in comparison to independent observation-based data and to the FFNN reconstruction. The retrospective prediction for the years 2021-2022 retained intra-seasonal to interannual variations of fCO_2 as those in the reconstruction time series and no large systematic bias has been observed between the two across all ocean provinces. The closeness between the predicted and reconstructed global net ocean budget implies that, when used as input to an atmospheric transport model, the prediction removes an appropriate mass of carbon from the simulated atmosphere: this is an important asset for greenhouse gas monitoring.

The latest model version, FFNNv2022, was ultimately used to predict fCO_2 from January 2022 to August 2023, i.e., up to 20 months beyond the coverage of its training dataset. This study also exemplified the assessment of air-sea CO_2 fluxes ($fgCO_2$) generated from the predicted fCO_2 in the years 2022-2023 over the eastern tropical Pacific, where regional CO_2 gas exchanges greatly vary with El Niño-Southern Oscillation (ENSO) conditions and thus affect substantially on interannual variability of the global net sink. The year 2022 has been predicted with persistently high fCO_2 (strong CO_2 outgassing to the atmosphere) in response to the maintenance of La Niña since summer 2020. A remarkable reduction in the tropical Pacific CO_2 source in August 2023 relative to the year before coincides with the weakening of the cooling phase. Recent discussions about the interaction between the ocean and climate have largely put attention on the El Niño revisits, their high possibility in triggering more extreme heat worldwide, and further impacts on the marine carbon cycle early at the end of 2023 onwards. However, already in June 2023 as exceptional surface ocean warming and extraordinarily low wind intensity fall out historical records over the north-eastern Atlantic ocean, we have found an anomalous reduction in CO_2 uptake setting this regional sink back to its magnitude in the 2000s. These results emphasise critical needs and open the possibility to derive monthly predictions for global surface ocean maps of numerous variables driven by fCO_2, including air-sea fluxes, seawater pH, and dissolved inorganic carbon, as the reconstruction quality of fCO_2 drives that of the other variables (Chau et al., 2022a, 2022b). The new datasets for the year 2022 (January) to 2023 (August) are available via the LSCE/IPSL data center (see Section Data availability) and are updated each month. This demonstration of an operational service will be extended at an increased horizontal resolution, following the current development of the reference CMEMS-LSCE-FFNN reconstructions (Chau et al., 2023).

Data availability

Data provided in this research are available for use with open access granted by the French LSCE/IPSL Data Center (`https://dods.lsce.ipsl.fr/invsat/FFNN_low-latency/`).

Acknowledgments

We acknowledge funding support by the MOB TAC project of the European Copernicus Marine Environment Monitoring Service (CMEMS, `https://marine.copernicus.eu/about/producers/mob-tac`, last access: 20/9/2023). SOCAT is an international effort endorsed by the International Ocean Carbon Coordination Project (IOCCP), the Surface Ocean Lower Atmosphere Study (SOLAS) and the Integrated Marine Biogeochemistry and Ecosystem Research program (IMBER), to deliver a uniformly quality-controlled surface ocean CO_2 database. The data center LSCE/IPSL has offered data repository and access. We thank François-Marie Bréon for the tool development of xCO$_2$ extrapolation and comments on the first manuscript version and we thank Cédric Bacour for his help in running the extrapolation tool.

References

Bakker, D., Alin, S., Becker, M., Bittig, H., Castaño-Primo, R., Feely, R. A., ... others (2022). *Socat version 2022 for quantification of ocean co$_2$ uptake.* Retrieved from `https://socat.info/index.php/version-2022/` doi: https://doi.org/10.25921/1h9f-nb73

Bakker, D., Alin, S., Castaño-Primo, R., Margot, C., Gritzalis, T., Kozyr, A., ... others (2021). *Socat version 2021 for quantification of ocean co$_2$ uptake.* Retrieved from `https://socat.info/index.php/version-2021/`

Bakker, D., Alin, S. R., Bates, N., Becker, M., Feely, R. A., Gkritzalis, T., ... others (2023). *Surface ocean co$_2$ atlas database version 2023 (socatv2023).* doi: https://doi.org/10.25921/r7xa-bt92

Bakker, D., Pfeil, B., Landa, C. S., Metzl, N., O'Brien, K. M., Olsen, A., ... Xu, S. (2016). A multi-decade record of high-quality $f$co$_2$ data in version 3 of the surface ocean co$_2$ atlas (socat). *Earth System Science Data*, *8*(2), 383–413. Retrieved from `https://essd.copernicus.org/articles/8/383/2016/` doi: 10.5194/essd-8-383-2016

Bates, N. R., Astor, Y. M., Church, M. J., Currie, K., Dore, J. E., González-Dávila, M., ... Santana-Casiano, J. M. (2014). A time-series view of changing surface ocean chemistry due to ocean uptake of anthropogenic co$_2$ and ocean acidification. *Oceanography*, *27*(1), 126–141.

Canadell, J. G., Monteiro, P. M., Costa, M. H., Da Cunha, L. C., Cox, P. M., Alexey, V., ... others (2021). Global carbon and other biogeochemical cycles and feedbacks in climate change 2021: The physical science basis. contribution of working group i to the sixth assessment report of the intergovernmental panel on climate change. Cambridge University Press. doi: 10.1017/9781009157896.007

Chau, T. T. T., Gehlen, M., & Chevallier, F. (2022a, December). *Global ocean surface carbon product* (Research Report No. CMEMS-MOB-QUID-015-008). Le Laboratoire des Sciences du Climat et de l'Environnement. Retrieved from `https://hal.archives-ouvertes.fr/hal-02957656` (Quality Information Document) doi: 10.48670/moi-00047

Chau, T. T. T., Gehlen, M., & Chevallier, F. (2022b). A seamless ensemble-based reconstruction of surface ocean $p\mathrm{co}_2$ and air–sea co_2 fluxes over the global coastal and open oceans. *Biogeosciences*, *19*(4), 1087–1109. Retrieved from `https://bg.copernicus.org/articles/19/1087/2022/` doi: 10.5194/bg-19-1087-2022

Chau, T. T. T., Gehlen, M., Metzl, N., & Chevallier, F. (2023). Cmems-lsce: A global 0.25-degree, monthly reconstruction of the surface ocean carbonate system. *Earth System Science Data Discussions*, *2023*, 1–52. doi: 10.5194/essd-2023-146

Cooley, S., Schoeman, D., Bopp, L., Boyd, P., Donner, S., Ito, S.-i., ... others (2022). Oceans and coastal ecosystems and their services. In *Ipcc ar6 wgii*. Cambridge University Press.

Doney, S. C., Busch, D. S., Cooley, S. R., & Kroeker, K. J. (2020). The impacts of ocean acidification on marine ecosystems and reliant human communities. *Annual Review of Environment and Resources*, *45*(1).

Fay, A. R., & McKinley, G. A. (2014). Global open-ocean biomes: mean and temporal variability. *Earth System Science Data*, *6*(2), 273–284. Retrieved from `https://essd.copernicus.org/articles/6/273/2014/` doi: 10.5194/essd-6-273-2014

Friedlingstein, P., O'Sullivan, M., Jones, M. W., Andrew, R. M., Gregor, L., Hauck, J., ... Zheng, B. (2022). Global carbon budget 2022. *Earth System Science Data*, *14*(11), 4811–4900. Retrieved from `https://essd.copernicus.org/articles/14/4811/2022/` doi: 10.5194/essd-14-4811-2022

Gallego, M., Timmermann, A., Friedrich, T., & Zeebe, R. E. (2018). Drivers of future seasonal cycle changes in oceanic pco 2. *Biogeosciences*, *15*(17), 5315–5327.

Gregor, L., & Gruber, N. (2021). Oceansoda-ethz: a global gridded data set of the surface ocean carbonate system for seasonal to decadal studies of ocean acidification. *Earth System Science Data*, *13*(2), 777–808. Retrieved from `https://essd.copernicus`

`.org/articles/13/777/2021/` doi: 10.5194/essd-13-777-2021

Gregor, L., Lebehot, A. D., Kok, S., & Scheel Monteiro, P. M. (2019). A comparative assessment of the uncertainties of global surface ocean CO_2 estimates using a machine-learning ensemble (csir-ml6 version 2019a) – have we hit the wall? *Geoscientific Model Development*, *12*(12), 5113–5136. Retrieved from `https://gmd.copernicus.org/articles/12/5113/2019/` doi: 10.5194/gmd-12-5113-2019

Gruber, N., Bakker, D. C., DeVries, T., Gregor, L., Hauck, J., Landschützer, P., ... Müller, J. D. (2023). Trends and variability in the ocean carbon sink. *Nature Reviews Earth & Environment*, *4*(2), 119–134.

Gruber, N., Landschützer, P., & Lovenduski, N. S. (2019). The variable southern ocean carbon sink. *Annual review of marine science*, *11*, 159–186.

Hopkins, F. E., Suntharalingam, P., Gehlen, M., Andrews, O., Archer, S. D., Bopp, L., ... others (2020). The impacts of ocean acidification on marine trace gases and the implications for atmospheric chemistry and climate. *Proceedings of the Royal Society A*, *476*(2237), 20190769.

Janssens-Maenhout, G., Pinty, B., Dowell, M., Zunker, H., Andersson, E., Balsamo, G., ... others (2020). Toward an operational anthropogenic co 2 emissions monitoring and verification support capacity. *Bulletin of the American Meteorological Society*, *101*(8), E1439–E1451.

Landschützer, P., Gruber, N., & Bakker, D. C. (2016). Decadal variations and trends of the global ocean carbon sink. *Global Biogeochemical Cycles*, *30*(10), 1396–1417.

Landschützer, P., Ilyina, T., & Lovenduski, N. S. (2019). Detecting regional modes of variability in observation-based surface ocean pco_2. *Geophysical Research Letters*, *46*(5), 2670–2679.

Regnier, P., Resplandy, L., Najjar, R. G., & Ciais, P. (2022). The land-to-ocean loops of the global carbon cycle. *Nature*, *603*(7901), 401–410.

Rödenbeck, C., Bakker, D. C. E., Gruber, N., Iida, Y., Jacobson, A. R., Jones, S., ... Zeng, J. (2015). Data-based estimates of the ocean carbon sink variability – first results of the surface ocean pco_2 mapping intercomparison (socom). *Biogeosciences*, *12*(23), 7251–7278. Retrieved from `https://bg.copernicus.org/articles/12/7251/2015/` doi: 10.5194/bg-12-7251-2015

Rödenbeck, C., Keeling, R. F., Bakker, D. C., Metzl, N., Olsen, A., Sabine, C., & Heimann, M. (2013). Global surface-ocean pco_2 and sea–air co_2 flux variability from an observation-driven ocean mixed-layer scheme. *Ocean Science*, *9*(2), 193–216.

Rustogi, P., Landschützer, P., Brune, S., & Baehr, J. (2023). The impact of seasonality on the annual air-sea carbon flux and its interannual variability. *npj Climate and Atmospheric Science*, *6*(1), 66.

Takahashi, T., Sutherland, S. C., Sweeney, C., Poisson, A., Metzl, N., Tilbrook, B., ... others (2002). Global sea–air co2 flux based on climatological surface ocean pco2, and seasonal biological and temperature effects. *Deep Sea Research Part II: Topical Studies in Oceanography*, *49*(9-10), 1601–1622.

Geophysical Research Letters

Supporting Information for

Global analysis of surface ocean CO_2 fugacity and air-sea fluxes with low latency

T. T. T. Chau[1], F. Chevallier[1], and M. Gehlen[1]

[1]Laboratoire des Sciences du Climat et de l'Environnement, LSCE/IPSL, CEA-CNRS-UVSQ, Université Paris-Saclay, F-91191 Gif-sur-Yvette, France

Contents of this file

1. Evaluation and analysis for surface ocean CO_2 fugacity and air-sea fluxes

1.1. Quality assessment for regional reconstruction and prediction of CO_2 fugacity (fCO_2)

In reconstruction mode (1985-2020), FFNNv2021 and FFNNv2 models perform with good skill over many ocean provinces (Figures 2, S3, and S5). Subtropical and tropical provinces (i.e., 3.NA-PS, 5.SA, 7.NP-PS, 8.PEQU-W, 10.SP, and 12.SIO) have the highest scores (RMSD < 14 µatm and r^2 > 0.74). Interestingly, these sub-basins are not dominant in data density compared to subpolar regions (2.NA-SS and 6.NP-SS) for the northern hemisphere and to the southern ocean (13.SO-SS) for the southern hemisphere (Figure 2). Data-rich provinces involve many observations distributed in coastal bands or in ocean upwelling systems with substantial fCO_2 inter-annual variations. These data put high weight on the calculated model-data mismatch (Figures S5 and S6). The model tends to get high biases from SOCAT data outliers (Figure S3), i.e., data beyond the 95% confidence interval ([279, 443] µatm) of the full data range. Overestimates of fCO_2 with a model-data bias greater than 100 µatm are distributed along the Arctic (1.ARC) and the subpolar-polar regions (2.NA-SS, 6.NP-SS, and 14.SO-ICE) (Figure S3 and Figure S5). Most of the poor estimates of fCO_2 belong to the coastal sector of these regions (Figure S5) where fCO_2 is characterized with high variability driven by multiple and complex physical and biological conditions (Feely et al., 2008; Bakker et al., 2016; Chavez et al., 2018; Chau et al., 2022). RMSD ranges from 21.1 µatm to 40 µatm and r^2 is between 0.57 and 0.76 over these regimes. In contrast, the FFNN models underestimate SOCAT fCO_2 at the right tail of its global distribution. Most of these data belong to the coastal sectors of NA-SS and NP-SS or are found in PEQU-E and NIO (see further analysis in Chau et al. (2022). Among these provinces, the eastern equatorial Pacific (9.PEQU-E) yields the largest RMSD (~27 µatm). Nevertheless, the reconstruction of the interannual variability of fCO_2 over PEQU-E has an r^2 of 0.71.

Despite general good performance as analyzed in the main manuscript, FFNNv2021 shows the poorest one-year prediction in 2021 relative to the 1985-2020 reconstruction skill in ARC (RMSD: 49.1 µatm vs 40 µatm; r^2: 0.25 vs 0.57), in AEQU (RMSD: 34.2 µatm vs 19.96 µatm; r^2: 0.36 vs 0.57), and in PEQU-E (RMSD: 37.2 µatm vs 27 µatm; r^2: 0.55 vs 0.71). The FFNNv2022 model reconstruction in 2021 benefits from more than 919 additional data (411 data points in the year 2021), resulting in an improvement in the fCO2 estimates in 2021 over the Arctic: the RMSD reduces to 41.8 µatm and r^2 rises up to 0.35 (Figure S7). In 2022, the FFNNv2022 model scores slightly better in one-year prediction (RMSD = 37.0 µatm and r^2 = 0.60) relative to the FFNNv2021 two-year prediction (RMSD = 37.7 µatm and r^2 = 0.56). To a smaller extent, this improvement holds for the equatorial Atlantic (4.AEQU) and the eastern equatorial Pacific (9.PEQU-E). For instance, the FFNNv2021 prediction (RMSD = 34.2 µatm and r^2 = 0.36) in AEQU in 2021 shows similar skill scores compared to the FFNNv2022 reconstruction (RMSD = 32.9 µatm and r^2 = 0.43). By contrast, the two model predictions perform well in 2022 (RMSD < 17.5 µatm and r^2 < 0.6), knowing that the evaluation data in SOCATv2023 in the years 2021 and 2022 do not have the same quantity and distribution over AEQU as well as other ocean provinces (Table S4 and Figure S5). For both reconstruction and prediction modes, the two time series of the mean fCO_2 derived from the two models deviate in interannual variability of fCO_2 in the equatorial Atlantic (Figure S6). Over the equatorial Pacific (9.PEQU-E), FFNNv2022 predicts fCO_2 in 2022 with a high deviation from SOCAT data (RMSD = 47.1 µatm) but reproduces its temporal variations well (r^2 = 0.76). FFNNv2021 makes the two-year prediction (RMSD = 45.1 µatm and r^2 = 0.77) marginally more precise than the latest model. The contradictory effects observed in the two FFNN performances over the tropical regions (4.AEQU and 9.PEQU-E) may derive from the discrepancy in SOCAT data used for model fits from one to another version; e.g., SOCATv2022 removed 234 [164] data from the previous version over AEQU [PEQU-E] for the period 1985-2020 (7% [2%] of the total data in this region) and added 116 [180] data for the year 2021 (Figures S2 and S7 and Table S4).

1.2. Computation of air-sea fluxes ($fgCO_2$)

An air–sea flux density of CO_2 is calculated in molC.m^{-2}.yr^{-1} by using the formulation as follows,

$$fgCO_2 = K \times dpCO_2 = k \times L \times (1 - f_{ice}) \times (pCO_2^{air} - pCO_2^{sea}), \quad (1)$$

where K is the gas transfer coefficient and $dpCO_2$ is the air-sea difference in partial pressure of CO_2 (pCO_2). K is the product of gas transfer velocity (k), temperature-dependent solubility of CO_2 (L), and sea ice coverage ratio (f_{ice}). L is estimated with sea surface temperature (Weiss, 1974) while the computation of k replies on a quadratic dependence of 10-m wind speed (Ho et al., 2006; Wanninkhof., 2014) and a scaling to match the global mean k of 16.5 cm.h^{-1} (Naegler, 2009). The derivation of atmospheric partial pressure of CO_2 (pCO_2^{air}) comes from CO_2 mole fraction multiplied with total pressure in dry air conditions. pCO_2^{sea} is converted from FFNN fCO_2 following Körtzinger., (1999). Data products used in the air-sea flux calculation are presented in Table S1. Given flux density per grid cell ($fgCO_2^{(i)}$), an integration of CO_2 fluxes ($PgC.yr^{-1}$) over a region or the global ocean derives from

$$fgCO_2 = \sum_{i=1:N} fgCO_2^{(i)} \times A^{(i)}, \quad (2)$$

where $A^{(i)}$ is the area in m^2 of grid cell (i).

1.3. Multi-year time series of $\boldsymbol{fCO_2}$ and $\boldsymbol{fgCO_2}$

Figures S6 and S8 (right sector of the red vertical line) respectively show the time series of mean fCO_2 predicted with FFNNv2022 models and of $fgCO_2$ integrated over different provinces. fCO_2 predicted for 2022 continues to increase resulting in an increment of the global average of sea surface partial pressure of CO_2 (pCO_2^{sea}) of 2.9 µatm relative to the year 2021 (Table S5) and much higher than its global growth rate of 1.7 $\mu atm.yr^{-1}$ (2.0 $\mu atm.yr^{-1}$) estimated over the period 1985-2022 (2010s). The one-year increment in atmospheric pCO_2 (pCO_2^{air}) between the two years (2.5 µatm) is less than in pCO_2^{sea} implying a reduction in the global ocean uptake of CO_2 predicted for 2022 (2.25±0.5 $PgC.yr^{-1}$) compared to the previous year (2.36±0.43 $PgC.yr^{-1}$). When adjusting the estimated global net fluxes with the riverine outgassing of CO_2 of 0.65 $PgC.yr^{-1}$ (Regnier et al., 2022) and the total ocean surface area (FFNNv2022 data covers 95% of the global ocean), one obtains the estimates of anthropogenic ocean carbon uptake about 3.13±0.46 $PgC.yr^{-1}$ and 3.02±0.52 $PgC.yr^{-1}$ in 2021 and 2022, respectively. The non-increasing imprint in the ocean sink of anthropogenic CO_2 found in this study is consistent with the 2022 projection proposed by Friedlingstein et al, (2022): the anthropogenic ocean sink in 2021 was 2.9±0.4 $PgC.yr^{-1}$ remains unchanged for the year 2022. This evidence supports the hypothesis that the persistence of cooling climate patterns (La Niña conditions) weakened CO_2 ocean uptake in 2021-2022 (high peaks appeared in mid-2022, Figure S9). For January to August in 2023, FFNNv2022 predicts a global net flux of 2.45±0.56 $PgC.yr^{-1}$ (w.r.s.t., 3.23±0.59 $PgC.yr^{-1}$ for anthropogenic uptake) higher than the 8-month net flux in 2022 of 2.17±0.50 $PgC.yr^{-1}$ (w.r.s.t., 2.94±0.53 $PgC.yr^{-1}$ for anthropogenic uptake).

1.4. Substantial intra- to inter-annual changes of $\boldsymbol{fCO_2}$ and air-sea fluxes ($\boldsymbol{fgCO_2}$) at the eastern equatorial Pacific (EEP) driven by the El Niño Southern Oscillation (ENSO)

The ENSO phenomenon does not only constrain ocean CO_2 outgassing at the tropical Pacific air-sea interface but also strongly affects the global net CO_2 uptake (Rödenbeck et al., 2015; Chau et al., 2022; Friedlingstein et al., 2022). In El Niño conditions, warmer surface temperature weakens vertical upwelling of subsurface water rich in dissolved inorganic carbon (DIC) and nutrients, therefore, El Niño leads to lower surface partial pressure of CO_2 (Feely et al., 2006; Wang et al., 2015). A decrease of fCO_2 reached 410 µatm and the intra-annual variation of fCO_2 was as large as 40 µatm in the year 2015 (Figure S6) as the strongest El Niño events of the last decade happened (Figure S9a). The dampening fCO_2 resulted in a reduction of the EEP source of CO_2 and thus an enhancement in the global ocean CO_2 uptake (Figure S8). The net flux excessed -0.15±0.03 PgC.yr^{-1} in 2015/2016 while the EEP normally released an average source of CO_2 of -0.31±0.02 PgC.yr^{-1} in the last decade. The spatial pattern in Figure S9bc confirms that the El Niño events spreading until the 2016 summer probably reduced fCO_2 below 400 µatm ($fgCO_2$ < -0.5 molC.m^{-2}.yr^{-1}) around 90°W and 150°W westward. Later in this period, the opposite conditions - La Niña - triggered in the 2017 summer became dominant and fCO_2 was, for the first time, rising over 460 µatm in the 2018 spring. La Niña has turned back and governed since the year 2020 (Figure S9a). The cooling phase persisted in 2021 and reached its maximum in the 2022 spring-summer. Anomalies in fCO_2 enhancement have been found throughout the year 2021 (Figure S9(b,c)). Likewise, FNNNv2022 correspondingly projects extremely high fCO_2 exceeding 484 µatm ($fgCO_2$ < -2.5 molC.m^{-2}.yr^{-1}) in the eastern Niño3 and Niño4 sectors in the first half of 2022. By then, a reduction of fCO_2 is predicted according to the lessening cooling conditions.

2. Tables

Table S1. Input datasets used for reconstructions and prediction of surface ocean CO_2 fugacity (fCO_2) and air-sea fluxes ($fgCO_2$) in 1985-2023.

Variables	Notation	Product name	References
Measurements of CO_2 fugacity	fCO_2	Surface ocean CO2 ATlas (SOCAT): SOCATv2021, SOCATv2022 (last access 17/06/2022), and SOCATv2023 (last access 20/06/2023)	Bakker et al. (2021, 2022, 2023)
Sea surface temperature	SST	Copernicus Marine Service (CMEMS): SST_GLO_SST_L4_REP_OBSERVATIONS_010_011 (1985-2021) SST_GLO_SST_L4_NRT_OBSERVATIONS_010_001 (2022-2023)	Good et al. (2020)
Sea ice fraction	f_{ice}		
Sea surface salinity	SSS	CMEMS: MULTIOBS_GLO_PHY_S_SURFACE_MYNRT_015_013 (1993-2023)	Buongiorno et al. (2016); Droghei et al. (2018)
Sea surface height	SSH	CMEMS: SEALEVEL_GLO_PHY_L4_MY_008_047 (1993-2021) SEALEVEL_GLO_PHY_L4_NRT_OBSERVATIONS_008_046 (2022-2023)	Pujol et al. (2016, 2018)

Mixed layer depth	MLD	Estimating the Circulation and Climate of the Ocean project Phase II (ECCO2): cube92_latlon_quart_90S90N (1992-2022)	Menemenlis et al. (2008)
Chlorophyll-*a*	Chl-*a*	CMEMS: OCEANCOLOUR_GLO_BGC_L4_MY_009_104 (1998-2023)	Garnesson et al . (2019)
Atmospheric CO_2 mole fraction	xCO_2	CO_2 atmospheric inversion from the Copernicus Atmosphere Monitoring Service (CAMS): Surface: v20r2 (1985-2020) Satellite: FT21r2 (2021)	Chevallier et al. (2005, 2010); Chevallier. (2013)
pCO_2 climatology	pCO_2^{clim}	Lamont Doherty Earth Observatory (LDEO) climatology of sea surface partial pressure of CO_2	Takahashi et al. (2009)
Wind speed	U	ERA5 hourly data on single levels from 1959 to present (1985-2023)	Hersbach et al., (2020)
Total pressure	Ps		

Notes:

- Preprocessing for missing data in the reconstruction mode (before the 2000s):
  - SSS and CHL-*a* (MLD) are set to climatologies computed on the available data (in 1992-1997).
  - SSH is set to climatologies plus linear trends computed on the available data
- Preprocessing for missing data in the prediction mode (2022-2023):

  Input datasets for prediction are set to the same data resources as for reconstruction, these data are available within a few weeks behind real time. This condition is not met for the xCO_2 and MLD datasets that we use in 2023. For xCO_2, we extrapolated the original dataset (the atmospheric inversion of the Copernicus Atmosphere Monitoring Service for years 1985- 2022, Table S1), knowing the recent measurements of the atmospheric CO_2 mole fraction at the Mauna Loa Observatory, Hawaii (https://gml.noaa.gov/ccgg/trends/mlo.html, last access: 11/9/2023). For MLD, given the dominance of seasonality in its variability (Menemenlis et al. 2008, Zhang et al. 2018), we use the last 5-year climatology of the Estimating the Circulation and Climate of the Ocean project Phase II (ECCO2) data in the prediction mode.

Table S2. Indicators of ocean provinces (Figure S1) used in this study.

No	Ocean provinces	Remarks
0	Global ocean (GLO)	

1	Arctic (ARC)	Aggregated from Arctic, North Atlantic, and North Pacific ice biomes and the Barents Sea (biomes 1, 2, 3, and 4)
2	North Atlantic seasonally stratified (NA-SS)	Aggregated from North Atlantic subpolar and subtropical seasonally stratified biomes (biomes 5 and 6)
3	North Atlantic permanently stratified (NA-PS)	North Atlantic subtropical permanently stratified biome (biome 7)
4	Atlantic equatorial (AEQU)	Biome 8
5	South Atlantic (SA)	South Atlantic subtropical permanently stratified biome (biome 9)
6	North Pacific seasonally stratified (NP-SS)	Aggregated from North Pacific subpolar and subtropical seasonally stratified biomes (biomes 11 and 12)
7	North Pacific permanently stratified (NP-PS)	North Pacific subtropical permanently stratified biome (biome 13)
8	Pacific western equatorial (PEQU-W)	Biome 14
9	Pacific eastern equatorial (PEQU-E)	Biome 15
10	South Pacific (SP)	South Pacific subtropical permanently stratified biome (Biome 16)
11	Northern Indian Ocean (NIO)	Aggregated from the Arabian Sea, Bay of Bengal, and Equatorial Indian Ocean above the Equator (biomes 17, 18, and 19)
12	Southern Indian Ocean (SIO)	Aggregated from the Equatorial Indian Ocean blow the Equator and the South Indian Ocean (biomes 19 and 20)
13	Southern Ocean seasonally stratified (SO-SS)	Aggregated from Southern Ocean subpolar and subtropical seasonally stratified biomes (biomes 21 and 22)
14	Southern Ocean icea (SO-ICE)	Biome 23

Table S3. Comparison of CMEMS-LSCE-FFNN models (FFNNv2021 and FFNNv2022)

a) Summary of SOCAT data used for model runs and model evaluation

FFNN	Model fitting			Model evaluation				
	Target Data	Time span	Number of data	Target Data	Reconstruction		Prediction	
					Time span	Number of data	Time span	Number of data

v2021	SOCATv2021	1985-2020	306357	SOCATv2023	1985-2020	302255	2021-2022	109088602
v2022	SOCATv2022	1985-2021	311694		1985-2021	313163	2022	8602

b) Model evaluation between global reconstructions of fCO_2 [μatm] in 1985-2020 and between FFNNv2021 prediction and FFNNv2022 reconstruction (prediction) in 2021 (2022). Statistics include the number of SOCAT monthly gridded data (N), mean fCO_2 (μ), mean uncertainty (σ), and model-data misfit (RMSD) and coefficient of determination (r^2).

FFNN	Years											
	1985-2020				2021				2022			
	μ	σ	RMSD	r^2	μ	σ	RMSD	r^2	μ	σ	RMSD	r^2
v2021	361.6	8.7	19.1	0.78	395.2	11.4	24.3	0.74	397.8	12.2	23.1	0.75
v2022	361.5	8.5	19.1	0.78	395.7	10.9	23.3	0.76	398.5	11.3	22.6	0.76

Table S4. **Regional comparison (a) between FFNN model reconstructions of fCO_2 [μatm] in 1985-2020, (b) between FFNNv2021 prediction and FFNNv2022 reconstruction in 2021, and (c) between FFNN model predictions in 2022. Statistics include 1) the number (N) of monthly gridded data used in FFNN fits (SOCATv2021 and SOCATv2022) and in data evaluation (SOCATv2023, see values in brackets), 2) mean fCO_2 (μ), 3) mean uncertainty (σ), and 4) model-data misfit (RMSD), and 5) determination coefficient (r^2).**

No	Biome	FFNN	Years														
			1985-2020					2021					2022				
			N	μ	σ	RMSD	r^2	N	μ	σ	RMSD	r^2	N	μ	σ	RMSD	r^2
1	ARC	v2021	5043 (5646)	320.5	30.0	40.0	0.57	0 (411)	356.3	31.3	49.1	0.25	0 (225)	351.4	29.6	37.7	0.56
		v2022	5551	318.0	29.3	40.0	0.57	411	348.5	29.5	41.8	0.35	0	345.	27.5	37.0	0.60
2	NA-SS	v2021	57808 (55738)	339.8	8.0	23.1	0.76	0 (2350)	368.8	9.0	26.0	0.76	0 (2265)	373.6	10.1	24.6	0.74
		v2022	55714	339.9	7.7	23.1	0.76	2167	369.1	8.3	26.2	0.75	0	374.	9.1	24.0	0.75

			(5646)					(411)					(225)	6			
			(55738)					(2350)					(2265)	8			
3	NA-PS	v2021	37951 (37011)	364.5	5.3	13.9	0.74	0 (1161)	398.4	6.3	20.4	0.50	0 (1007)	401. 0	7.0	18.2	0.61
		v2022	36991 (37011)	364.5	5.1	13.8	0.75	945 (1161)	399.3	5.9	20.1	0.51	0 (1007)	402. 7	6.5	17.0	0.65
4	AEQU	v2021	3313 (3179)	376.9	10.0	20.0	0.57	0 (182)	400.2	12.8	34.2	0.36	0 (144)	403. 1	14.2	17.3	0.64
		v2022	3179 (3179)	376.0	10.0	19.9	0.57	116 (182)	400.5	13.2	32.9	0.43	0 (144)	404. 2	13.6	16.7	0.65
5	SA	v2021	6575 (6497)	369.6	7.9	13.2	0.79	0 (273)	398.5	9.5	14.3	0.55	0 (161)	401. 1	10.2	12.8	0.51
		v2022	6497 (6497)	369.7	7.6	12.9	0.80	212 (273)	401.9	9.2	12.4	0.59	0 (161)	404. 3	9.6	12.0	0.55
6	NP-SS	v2021	57531 (58165)	349.1	8.2	21.1	0.73	0 (2334)	378.9	10.1	28.3	0.76	0 (1495)	383. 1	11.1	31.0	0.62
		v2022	58161 (58165)	349.5	8.0	21.0	0.74	2147 (2334)	380.8	9.4	27.4	0.77	0 (1495)	385. 9	10.2	30.2	0.64
7	NP-PS	v2021	40176 (40300)	360.7	5.3	11.9	0.85	0 (1705)	397.0	7.1	16.4	0.76	0 (1608)	401. 3	8.4	13.2	0.78
		v2022	40287 (40300)	360.6	5.1	11.8	0.85	1443 (1705)	397.1	6.5	16.1	0.77	0 (1608)	401. 5	7.3	12.4	0.81
8	PEQU-W	v2021	14845 (14821)	366.6	6.1	11.2	0.72	0 (484)	407.2	9.2	11.2	0.76	0 (326)	411. 6	10.7	12.0	0.73
		v2022	14821 (14821)	366.6	6.0	11.2	0.72	430 (484)	407.8	8.2	11.1	0.74	0 (326)	411. 8	9.1	10.9	0.78
9	PEQU-E	v2021	9470 (9306)	415.7	9.9	27.0	0.71	0 (199)	460.0	14.4	37.2	0.55	0 (146)	462. 4	15.7	45.0	0.77
		v2022	9306 (9306)	415.5	9.7	26.9	0.71	180 (199)	459.8 9	13.1	35.2	0.59	0 (146)	461. 9	13.8	47.1	0.76
10	SP	v2021	21551 (20968)	363.1	9.0	11.9	0.86	0 (689)	398.4	11.9	10.2	0.85	0 (592)	399. 8	12.6	10.1	0.80
		v2022	20968 (20968)	363.5	8.8	11.8	0.87	605 (689)	399.3	11.3	9.8	0.86	0 (592)	400. 5	11.5	10.0	0.80
11	NIO	v2021	1335 (1335)	382.8	15.0	24.0	0.53	0 (0)	418.3	23.6	nan	nan	0 (0)	419. 8	24.4	nan	nan
		v2022	1335 (1335)	382.1	14.7	23.9	0.54	0 (0)	416.8	23.7	nan	nan	0 (0)	419. 7	23.4	nan	nan
12	SIO	v2021	4583 (4562)	357.2	9.3	10.8	0.88	0 (133)	392.6	14.1	11.2	0.80	0 (73)	394. 1	14.8	8.8	0.43
		v2022	4562 (4562)	356.7	9.0	10.8	0.88	133 (133)	392.8	13.8	12.0	0.81	0 (73)	394. 2	13.6	9.3	0.45

13	SO-SS	v2021	32819 (31424)	351.8	8.4	15.2	0.68	0 (777)	384.4	11.1	15.2	0.66	0 (400)	386.6	11.7	18.1	0.42
		v2022	31404 (31424)	351.6	8.6	15.1	0.69	624 (777)	384.7	10.6	15.2	0.67	0 (400)	386.9	11.2	17.9	0.44
14	SO-ICE	v2021	12266 (12277)	362.5	10.7	28.7	0.58	0 (193)	388.6	13.4	24.4	0.44	0 (142)	388.2	13.5	41.8	0.76
		v2022	12277 (12277)	362.9	10.6	28.6	0.59	185 (193)	388.7	12.7	22.2	0.47	0 (142)	388.2	13.0	40.9	0.78

Table S5. Area-integrated air-sea CO_2 fluxes ($fgCO_2$) derived from FFNNv2022 fCO_2 reconstruction in 1985-2021 and from FFNNv2022 predictions in 2022-2023. The units of $fgCO_2$ are in $PgC.yr^{-1}$. Area-averaged surface temperature (SST), 10-m wind speed (U), sea surface partial pressure of CO_2 (pCO_2^{sea}), air-sea pCO_2 difference ($dpCO_2$), and gas transfer coefficient (K) are provided for the global ocean and each ocean province (see province indicator in Figure S1).

No	Biome	Area [10^6 km^2]	Years	Variables					
				SST [°C]	U [ms^{-1}]	pCO_2^{sea} [µatm]	$dpCO_2$ [µatm]	K [$molC.m^{-2}.yr^{-1}.\mu atm^{-1}$]	$fgCO_2$ [$PgC.yr^{-1}$]
0	**GLO**	343.3	1985-2020	18.8	7.8	362.8±10.5	2.8	0.0526	1.583±0.341
			2021	19.0	7.9	397.1±13.0	6.0	0.0524	2.355±0.434
			2022	19.2	7.9	400.0±13.0	5.7	0.0528	2.249±0.495
			2023/01-08	19.1	7.8	401.5±14.1	7.0	0.0519	2.449±0.557
1	**ARC**	6.9	1985-2020	-0.5	7.3	324.9±33.3	50.3	0.0228	0.082±0.017
			2021	-0.1	7.5	355.5±34.2	55.9	0.026	0.107±0.020
			2022	-0.1	7.5	356.4±32.6	60.0	0.0281	0.106±0.017
			2023/01-08	-0.5	6.5	366.0±39.9	53.8	0.0137	0.077±0.015
2	**NA-SS**	15.9	1985-2020	11.8	9.2	341.2±9.5	30.4	0.0733	0.384±0.041
			2021	12.3	9.4	370.4±9.8	38.6	0.0750	0.503±0.045
			2022	12.5	9.3	376.1±10.4	37.0	0.0731	0.475±0.048
			2023/01-08	12.0	9.0	376.2±11.2	39.4	0.0697	0.467±0.052

3	**NA-PS**	22.2	1985-2020	25.1	7.0	365.7±5.9	0.8	0.0397	0.042±0.025
			2021	25.4	7.0	400.6±6.6	3.1	0.0389	0.064±0.027
			2022	25.4	6.9	403.6±7.0	3.5	0.0383	0.073±0.031
			2023/01-08	25.4	6.8	404.2±7.7	5.8	0.037	0.092±0.034
4	**AEQU**	8.5	1985-2020	26.9	5.5	377.2±12.5	-14.2	0.0254	-0.040±0.010
			2021	27.4	5.5	401.8±15.5	-1.9	0.0251	-0.009±0.017
			2022	27.2	5.5	405.9±15.5	-3.5	0.0245	-0.012±0.016
			2023/01-08	27.6	5.4	404.0±17.1	0.6	0.0241	-0.002±0.018
5	**SA**	19.5	1985-2020	22.6	7.2	371.0±8.5	-5.2	0.0419	-0.012±0.033
			2021	22.8	7.3	403.2±10.1	0.5	0.0423	0.049±0.048
			2022	22.8	7.2	405.6±10.6	-0.4	0.0406	0.036±0.047
			2023/01-08	23.5	7.1	411.0±11.8	-2.9	0.0405	0.024±0.059
6	**NP-SS**	24.7	1985-2020	12.7	8.7	350.8±10.2	21.4	0.0651	0.393±0.056
			2021	13.3	8.5	382.2±11.8	27.6	0.0618	0.476±0.060
			2022	13.6	8.6	387.6±12.0	26.4	0.0632	0.477±0.073
			2023/01-08	12.6	8.3	389.1±13.0	27.8	0.0589	0.436±0.078
7	**NP-PS**	40.2	1985-2020	26.3	7.0	361.7±6.1	2.9	0.0404	0.130±0.040
			2021	26.4	6.9	398.4±7.6	3.7	0.0388	0.152±0.053
			2022	26.5	6.8	402.8±8.2	2.5	0.0373	0.126±0.052
			2023/01-08	26.1	7.1	403.4±8.6	5.1	0.0412	0.176±0.069
8	**PEQU-W**	13.1	1985-2020	29.3	5.1	367.7±7.6	-7.9	0.0220	-0.023±0.010
			2021	29.4	5.2	409.0±9.4	-12.4	0.0222	-0.040±0.013
			2022	29.3	5.4	413.3±10.0	-14.0	0.0236	-0.052±0.016
			2023/01-08	29.5	5.2	412.1±10.7	-10.2	0.0227	-0.036±0.016
9	**PEQU-E**	15.1	1985-2020	26.3	5.9	416.8±10.8	-54.0	0.0292	-0.294±0.023
			2021	25.9	6.3	461.3±14.2	-60.8	0.0314	-0.350±0.030
			2022	25.6	6.4	463.5±15.0	-60.4	0.0328	-0.370±0.037

			2023/01-08	27.5	5.8	460.2±15.0	-55.7	0.0277	-0.297±0.036
10	**SP**	54.8	1985-2020	22.0	7.5	364.7±9.9	0.1	0.0470	0.103±0.117
			2021	22.1	7.6	400.6±12.4	2.6	0.0468	0.161±0.146
			2022	22.0	7.6	401.9±12.5	3.3	0.0464	0.166±0.146
			2023/01-08	22.8	7.5	405.0±13.3	2.2	0.0463	0.201±0.168
11	**NIO**	11.4	1985-2020	28.2	6.0	383.3±17.0	-21.7	0.0317	-0.113±0.042
			2021	28.5	6.0	418.1±25.8	-19.8	0.0305	-0.099±0.077
			2022	28.4	6.0	421.1±25.2	-20.1	0.0311	-0.104±0.075
			2023/01-08	28.6	6.0	421.3±23.8	-17.4	0.0324	-0.096±0.076
12	**SIO**	32.9	1985-2020	24.8	7.1	357.8±9.6	5.8	0.0421	0.187±0.064
			2021	25.0	7.2	394.0±14.8	7.1	0.0422	0.216±0.114
			2022	24.9	7.2	395.4±14.5	7.6	0.0423	0.223±0.119
			2023/01-08	25.3	7.1	397.9±13.8	8.1	0.0414	0.222±0.109
13	**SO-SS**	59.6	1985-2020	8.0	10.5	353.0±9.4	13.3	0.0951	0.721±0.185
			2021	8.2	10.7	386.2±11.6	18.0	0.0956	1.006±0.232
			2022	8.2	10.7	388.4±12.1	17.8	0.0955	0.980±0.269
			2023/01-08	8.7	10.6	391.7±13.4	17.8	0.0950	1.006±0.314
14	**SO-ICE**	17.3	1985-2020	-1.1	9.1	366.1±11.9	-5.0	0.0421	0.022±0.040
			2021	-1.0	9.1	392.3±14.0	5.2	0.0423	0.119±0.042
			2022	-1.0	9.5	394.4±14.6	4.7	0.0525	0.122±0.054
			2023/01-08	-0.7	9.4	392.3±14.7	11.1	0.0575	0.175±0.073

3. Figures

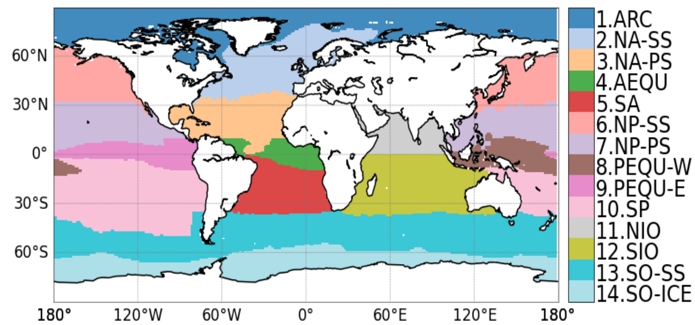

Figure S1. **Ocean provinces aggregated from the biomes used in the RECCAP2 project (source: https://github.com/RECCAP2-ocean/RECCAP2-shared-resources/tree/master/data/regions, last access: 20/3/2023). See Table S2 for the province indicator.**

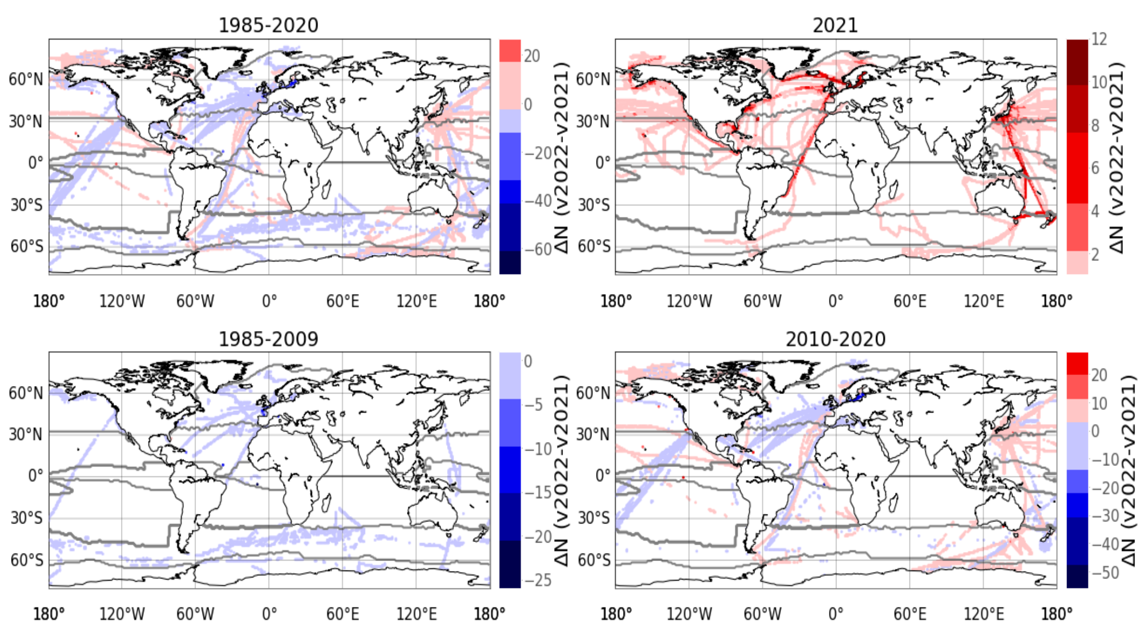

Figure S2. **Number of fCO_2 data (ΔN) added in (red) or removed from (blue) SOCATv2022 compared to SOCATv2021 for different time frames.**

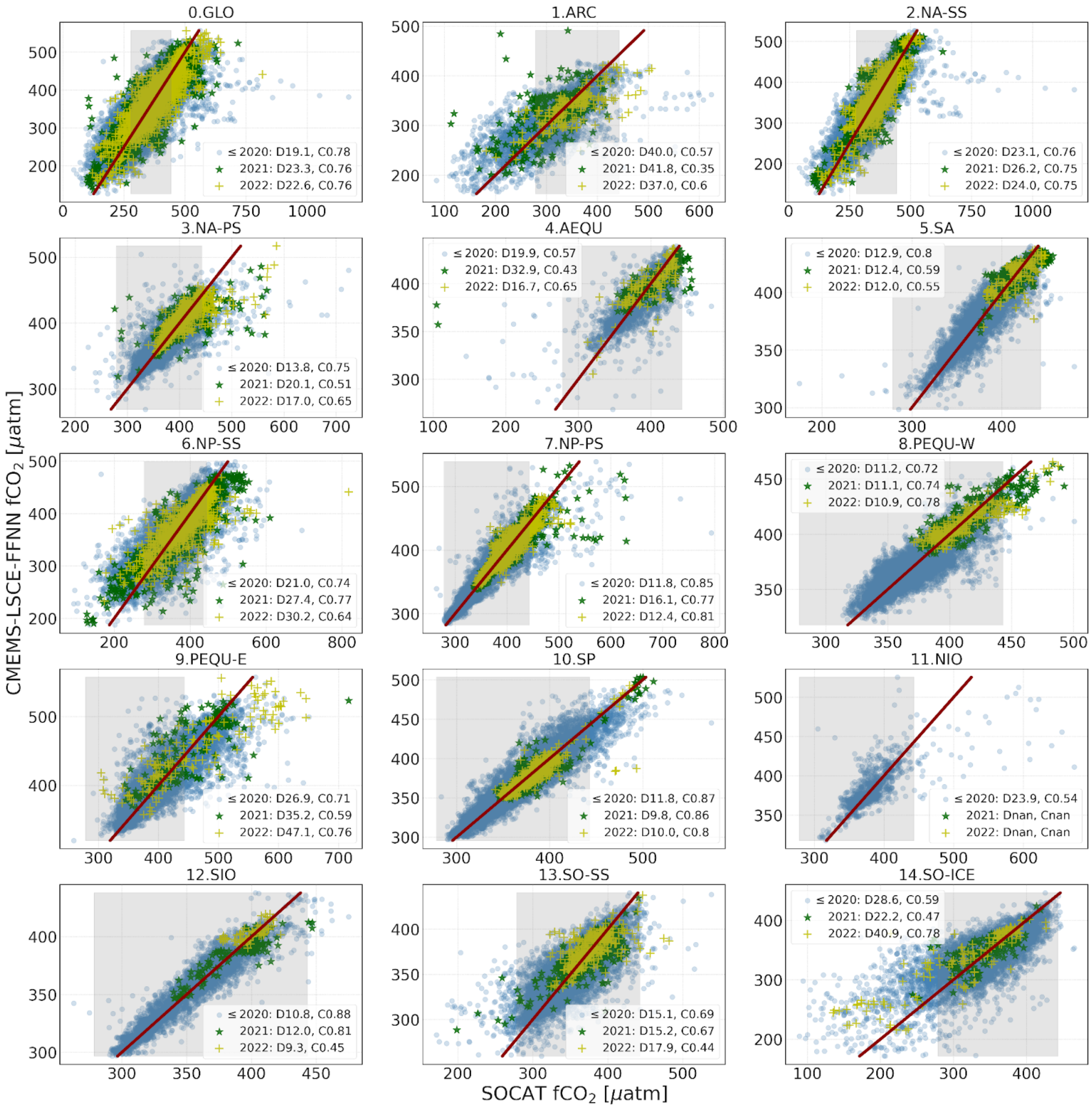

Figure S3. Scatter plots of FFNNv2022 versus SOCATv2023 *f*CO_2 [µatm] for 36-year reconstruction (1985-2020: points), 1-year reconstruction (2021: stars) and 1-year prediction (2022: pluses). Values of FFNNv2022 and SOCATv2023 data are shown in y- and x-axis, respectively. Light-grey rectangles mark the 95% SOCAT data range (i.e., [279, 443] µatm) over the global ocean in 1985-2021. Red lines represent the bisector corresponding to ideal model-data fits: objects above this line indicate FFNN overestimates of SOCAT *f*CO_2 and vice versa. Metrics for reconstruction and prediction in the legend are model-data standard deviation (D: RMSD) and correlation (C: r^2).

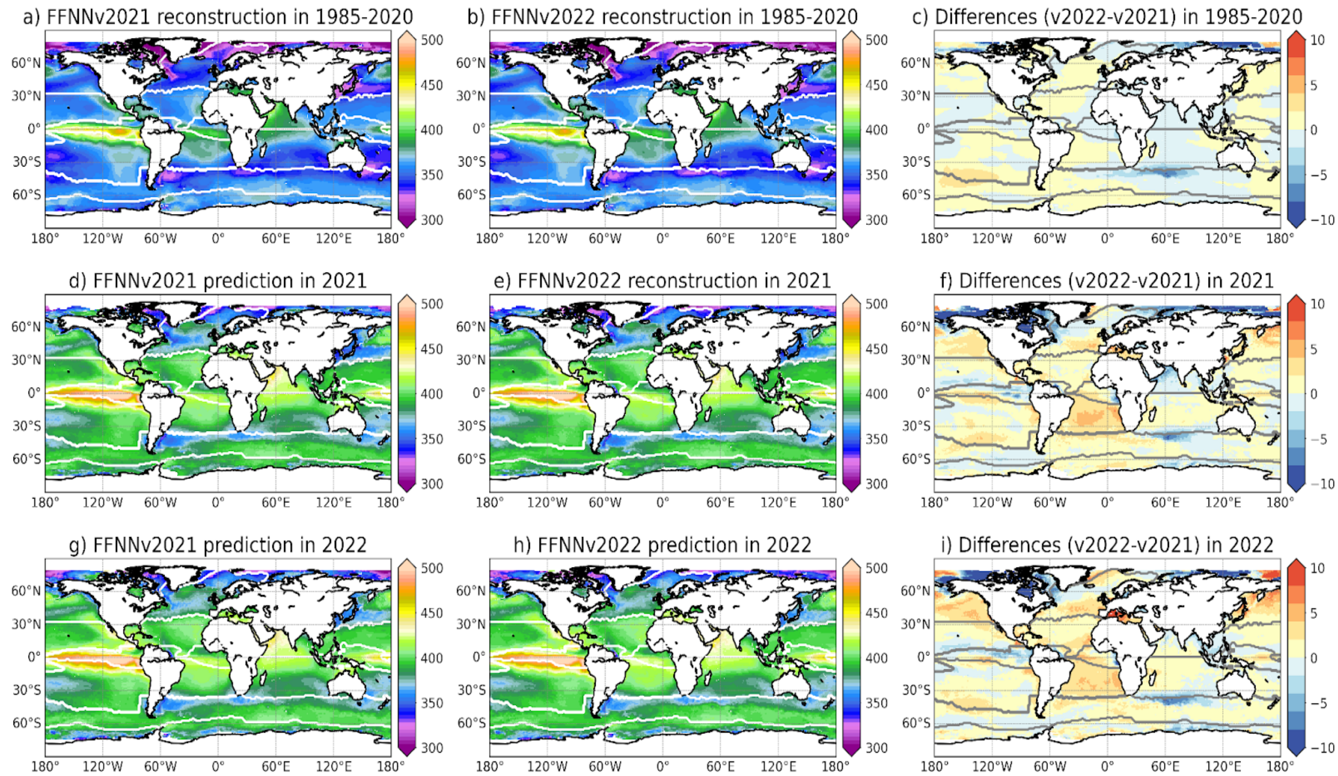

Figure S4. Spatial distribution of temporal means of *f*CO_2 derived from FFNNv2021 (left) and FFNNv2022 (middle) and their discrepancy (right).

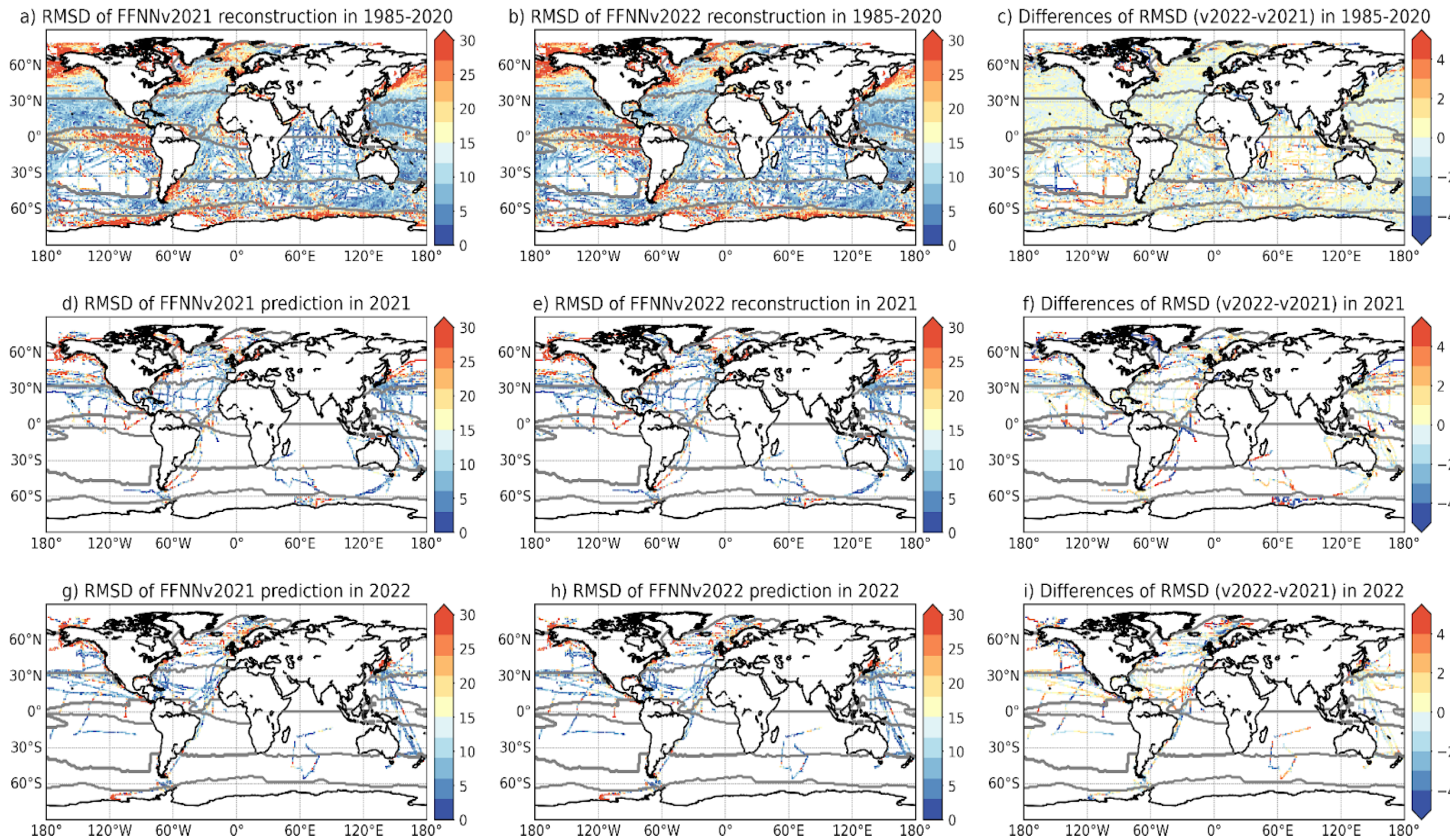

Figure S5. Spatial distribution of model-data deviation (RMSD): fCO_2 derived from FFNNv2021 (left) and FFNNv2022 (middle) and their RMSD difference (right). SOCATv2023 is used for this evaluation.

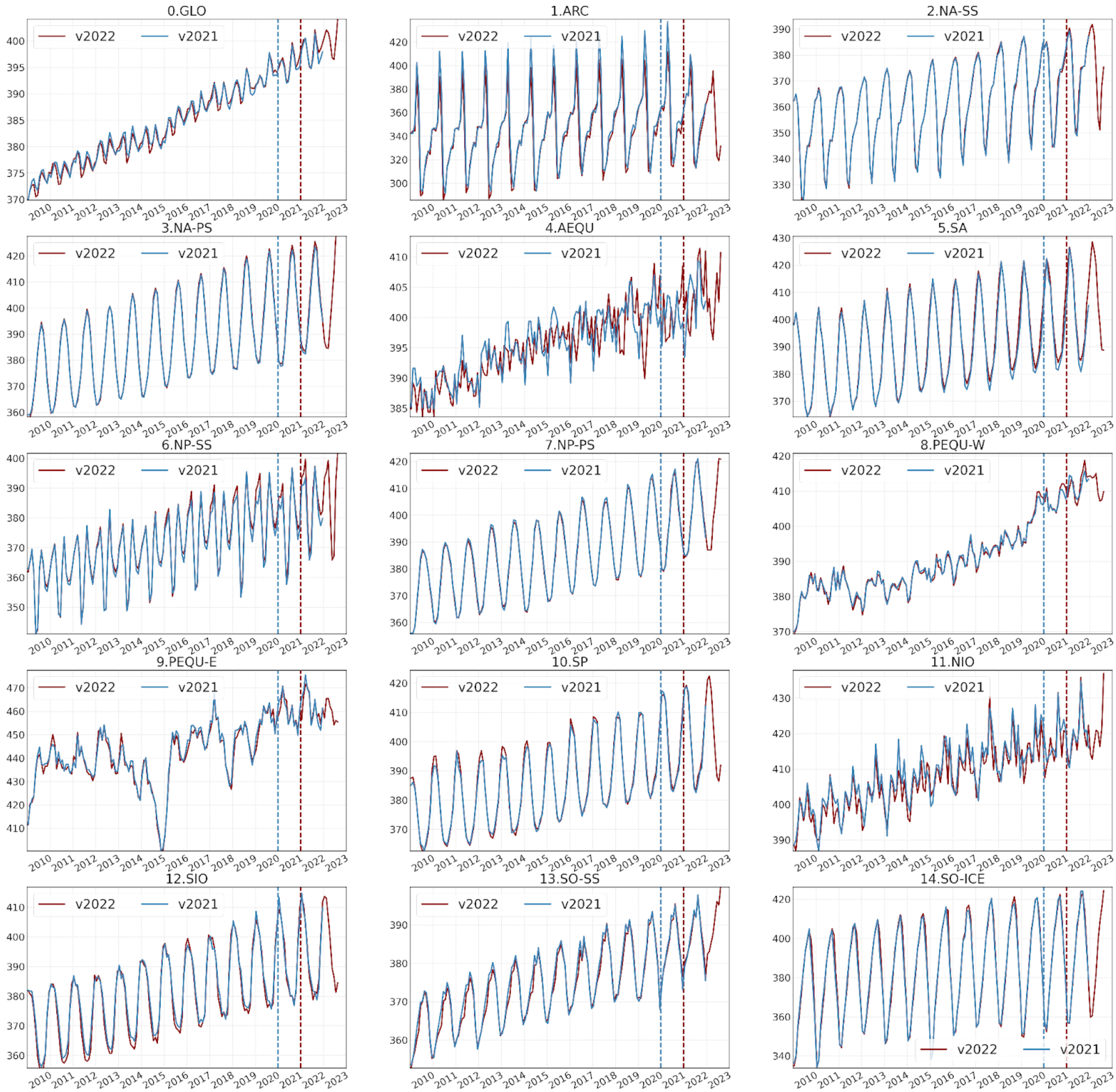

Figure S6. Time series of fCO$_2$ averaged over ocean provinces. Vertical dashed lines mark the starting date for model prediction (blue: FFNNv2021, red: FFNNv2022).

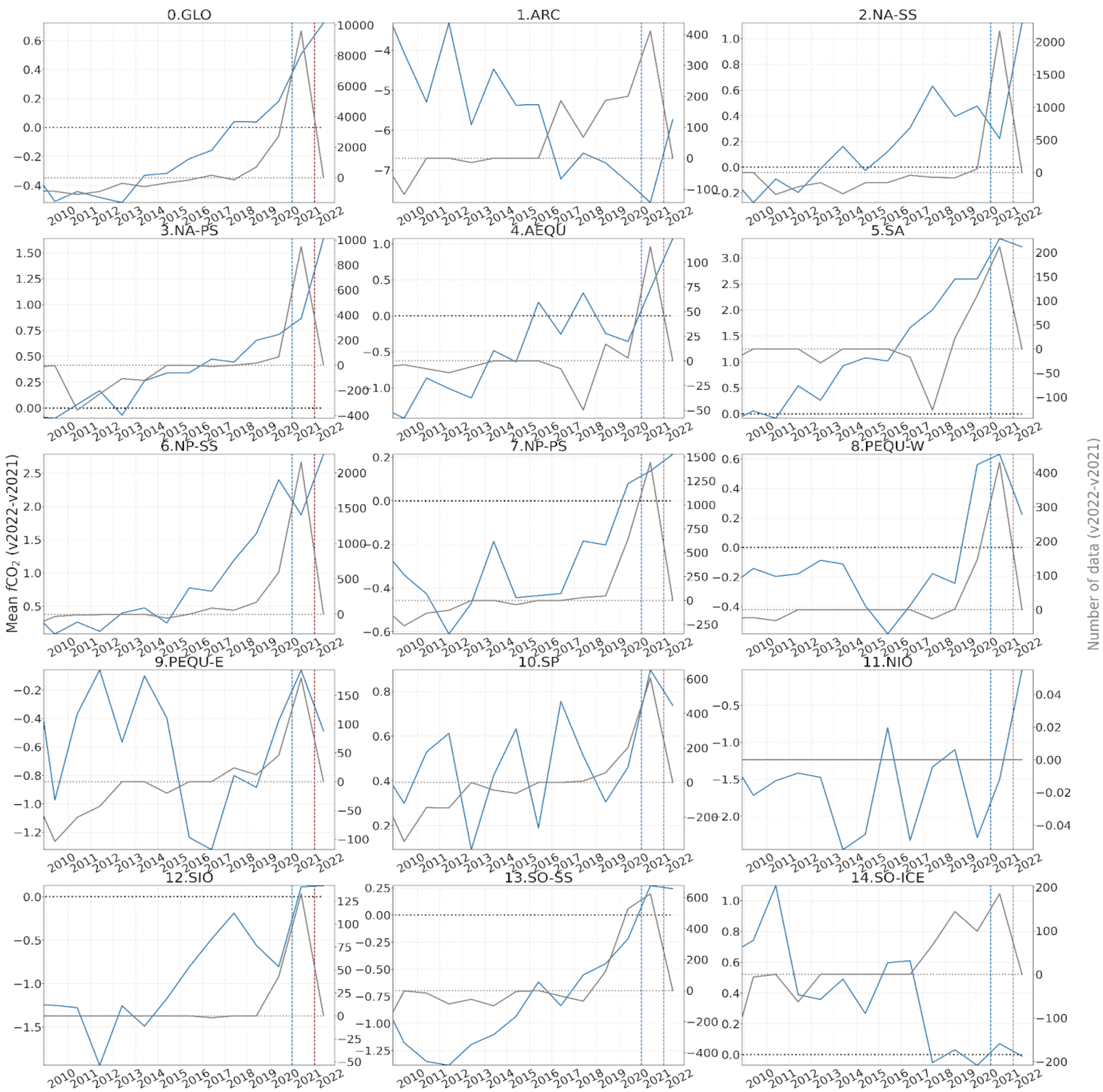

Figure S7. Time series of differences in *f*CO_2 (left y-axis) and number of SOCAT data (right y-axis). Vertical dashed line marks the starting date for prediction (FFNNv2021: blue, FFNNv2022: red).

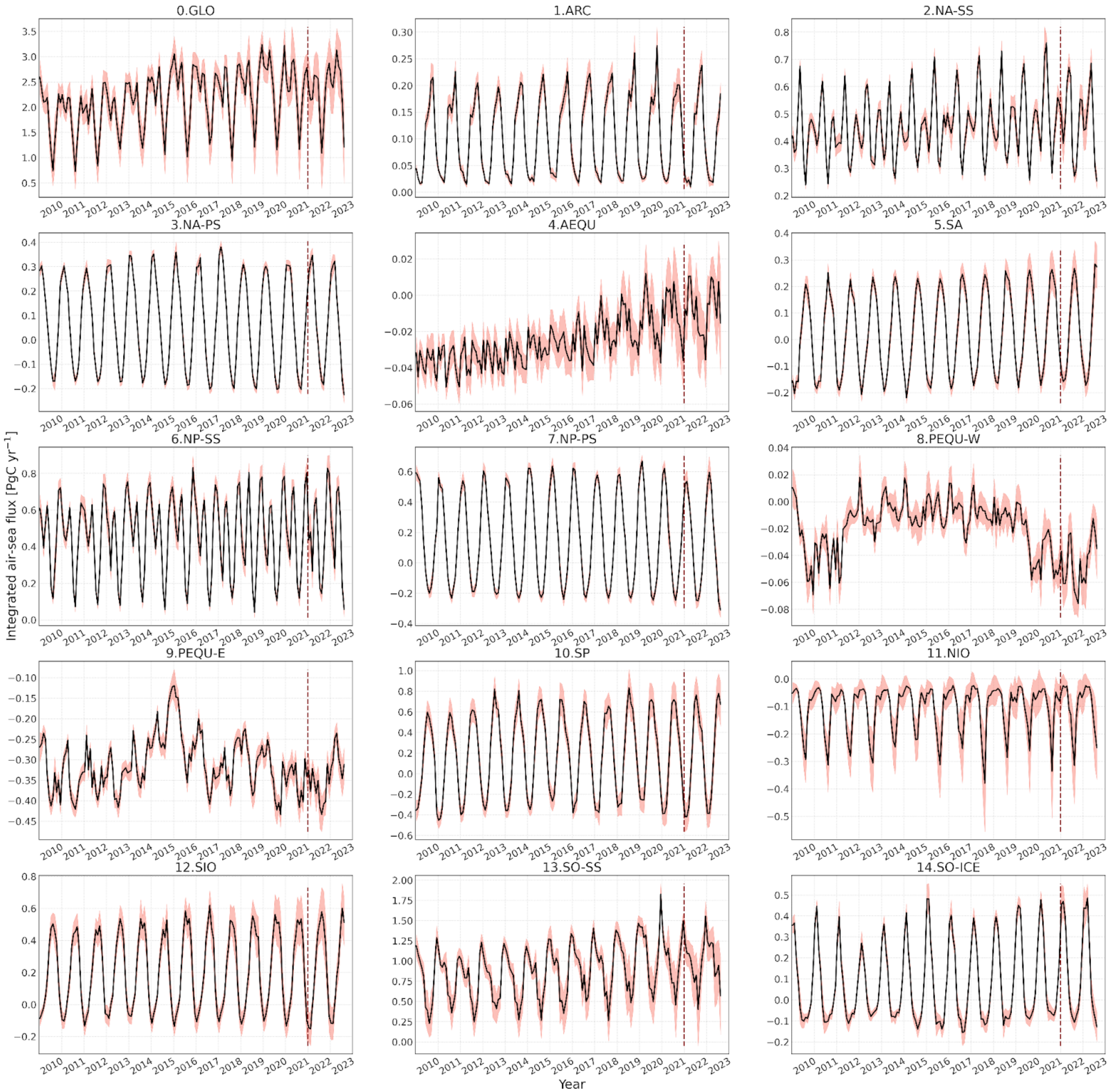

Figure S8. Time series of monthly air-sea fluxes integrated over ocean provinces [PgC.yr^{-1}]. Plain curve and shaded area represent model's best estimate and 1σ-uncertainty. Vertical dashed lines mark the starting date for FFNNv2022 prediction.

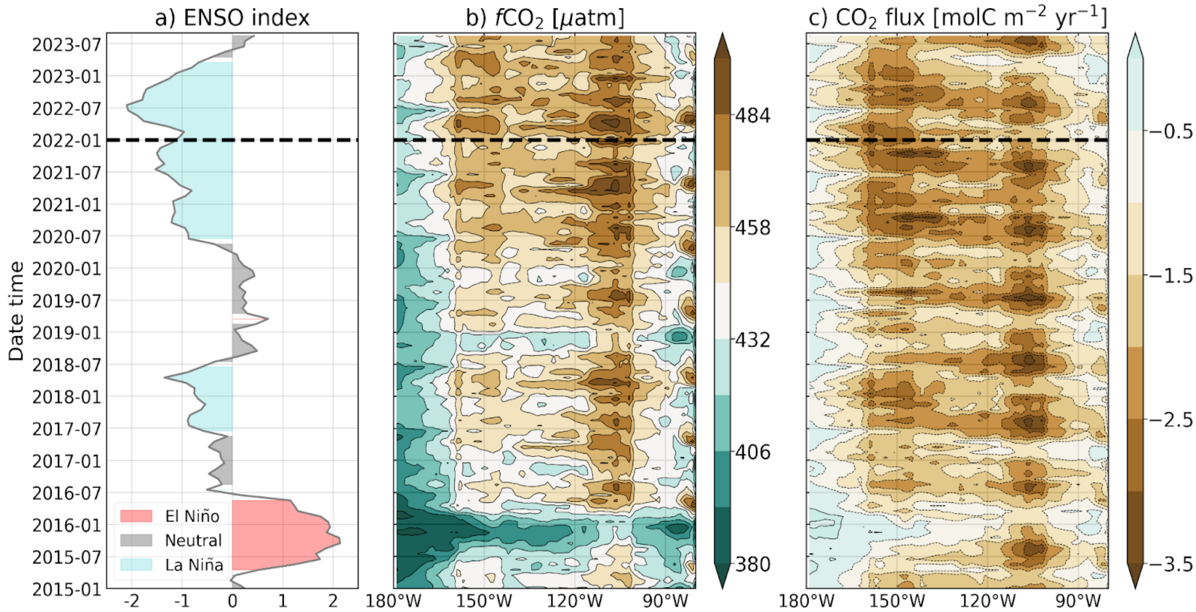

Figure S9. Illustration of the relationship between ENSO events (a) and FFNNv2022 fCO_2 (air-sea fluxes) variations (Hovmöller plots in b and c) over the eastern Equatorial Pacific (9.PEQU-E). ENSO events are plotted with the NOAA bi-monthly Multivariate El Niño/Southern Oscillation (ENSO) index ([https://psl.noa35.5, 50.5a.gov/enso/mei/](https://psl.noa35.5,%2050.5a.gov/enso/mei/), last access: 11/09/2023). The black horizontal dotted line marks the starting date for the FFNNv2022 prediction (January 2022).

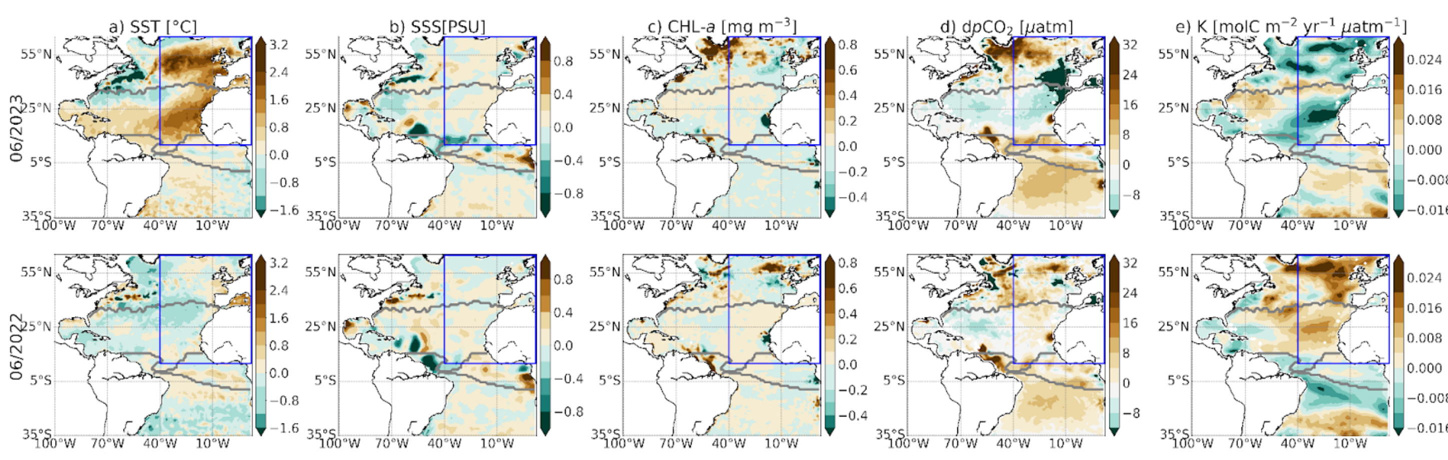

Figure S10. Anomalies of surface temperature (SST), salinity (SSS), Chlorophyll-*a* (CHL-*a*), air-sea pCO_2 difference (dpCO_2), gas transfer coefficient (K) over the Atlantic in June 2023 (top) and June 2022 (bottom) are computed by subtracting long-term trends and seasonal climatologies relative to the years 1985-2022. Blue box limits the region of interest where the extreme marine heat wave appeared in the northeastern Atlantic in June 2023.

References

Bakker, D., Alin, S., Becker, M., Bittig, H., Castaño-Primo, R., Feely, R. A., Gritzalis, T., Kadono, K., Kozyr, A., Lauvset, S. K., Metzl, N., Munro, D., Nakaoka, S.-i., Nojiri, Y., O'Brien, K., Olsen, A., Pfeil, B., Pierrot, D., Steinhoff, T., Sullivan, K., Sutton, A., Sweeney, C., Tilbrook, B., Wada13, C., Wanninkhof, R., Wranne, A. W., et al.: SOCAT version 2021 for quantification of ocean CO2 uptake, https://www.socat.info/wp-content/uploads/2022/06/2022_Poster_SOCATv2021_release.pdf, 2021.

Bakker, D., Alin, S., Becker, M., Bittig, H., Castaño-Primo, R., Feely, R. A., Gritzalis, T., Kadono, K., Kozyr, A., Lauvset, S. K., Metzl, N., Munro, D., Nakaoka, S.-i., Nojiri, Y., O'Brien, K., Olsen, A., Pfeil, B., Pierrot, D., Steinhoff, T., Sullivan, K., Sutton, A., Sweeney, C., Tilbrook, B., Wada13, C., Wanninkhof, R., Wranne, A. W., et al.: SOCAT version 2022 for quantification of ocean CO2 uptake, https://www.socat.info/wp-content/uploads/2022/06/2022_Poster_SOCATv2022_release.pdf, 2022.

Bakker, D., Alin, S. R., Bates, N., Becker, M., Feely, R. A., Gkritzalis, T., . . . others. Surface ocean co2 atlas database version 2023 (socatv2023). doi: https://doi.org/10.25921/r7xa-bt92, 2023.

Buongiorno Nardelli, B., R. Droghei, and R. Santoleri. Multi-dimensional interpolation of SMOS sea surface salinity with surface temperature and in situ salinity data, Remote Sens. Environ., 180, 392– 402, doi:10.1016/j.rse.2015.12.052, 2016.

Chau, T. T. T., Gehlen, M., and Chevallier, F.: A seamless ensemble-based reconstruction of surface ocean *p*CO_2 and air–sea CO_2 fluxes over the global coastal and open oceans, Biogeosciences, 19, 1087–1109, https://doi.org/10.5194/bg-19-1087-2022, 2022.

Chavez, F. P., Sevadjian, J., Wahl, C., Friederich, J., & Friederich, G. E. (2018). Measurements of pco2 and ph from an autonomous surface vehicle in a coastal upwelling system. Deep Sea Research Part II: Topical Studies in Oceanography, 151 , 137–146.

Chevallier, F.: On the parallelization of atmospheric inversions of CO_2 surface fluxes within a variational framework, Geosci. Model Dev., 6, 783–790, https://doi.org/10.5194/gmd-6-783-2013, 2013.

Chevallier, F., Fisher, M., Peylin, P., Serrar, S., Bousquet, P., Bréon, F.-M., Chédin, A., and Ciais, P.: Inferring CO_2 15 sources and sinks from satellite observations: Method and application to TOVS data, J. Geophys. Res. Atmos., 110, https://doi.org/https://doi.org/10.1029/2005JD006390, 2005.

Chevallier, F., Ciais, P., Conway, T. J., Aalto, T., Anderson, B. E., Bousquet, P., Brunke, E. G., Ciattaglia, L., Esaki, Y., Fröhlich, M., Gomez, A., Gomez-Pelaez, A. J., Haszpra, L., Krummel, P. B., Langenfelds, R. L., Leuenberger, M., Machida, T., Maignan, F., Matsueda, H., Morguí, J. A., Mukai, H., Nakazawa, T., Peylin, P., Ramonet, M., Rivier, L., Sawa, Y., Schmidt, M., Steele, L. P., Vay, S. A., Vermeulen, A. T., Wofsy, S., and Worthy, D.: CO_2 surface fluxes at grid point scale estimated from a global 21 year reanalysis of atmospheric measurements, J. Geophys. Res. Atmos., 115, https://doi.org/https://doi.org/10.1029/2010JD013887, 2010.

Droghei, R., Buongiorno Nardelli, B., and Santoleri, R.: A new global sea surface salinity and density dataset from multivariate observations (1993–2016), Frontiers in Marine Science, 5, 84, 2018.

Feely, R. A., Takahashi, T., Wanninkhof, R., McPhaden, M. J., Cosca, C. E., Sutherland, S. C., and Carr, M.-E. Decadal variability of the air-sea CO_2 fluxes in the equatorial Pacific Ocean, *J. Geophys. Res.*, 111, C08S90, doi:10.1029/2005JC003129, 2006.

Feely, R. A., Sabine, C. L., Hernandez-Ayon, J. M., Ianson, D., & Hales, B. (2008). Evidence for upwelling of corrosive" acidified" water onto the continental shelf. science, 320 (5882), 1490–1492.

Friedlingstein, P., O'Sullivan, M., Jones, M. W., Andrew, R. M., Gregor, L., Hauck, J., Le Quéré, C., Luijkx, I. T., Olsen, A., Peters, G. P., Peters, W., Pongratz, J., Schwingshackl, C., Sitch, S., Canadell, J. G., Ciais, P., Jackson, R. B., Alin, S. R., Alkama, R., Arneth, A., Arora, V. K., Bates, N. R., Becker, M., Bellouin, N., Bittig, H. C., Bopp, L., Chevallier, F., Chini, L. P., Cronin, M., Evans, W., Falk, S., Feely, R. A., Gasser, T., Gehlen, M., Gkritzalis, T., Gloege, L., Grassi, G., Gruber, N., Gürses, O., Harris, I., Hefner, M., Houghton, R. A., Hurtt, G. C., Iida, Y., Ilyina, T., Jain, A. K., Jersild, A., Kadono, K., Kato, E., Kennedy, D., Klein Goldewijk, K., Knauer, J., Korsbakken, J. I., Landschützer, P., Lefèvre, N., Lindsay, K., Liu, J., Liu, Z., Marland, G., Mayot, N., McGrath, M. J., Metzl, N., Monacci, N. M., Munro, D. R., Nakaoka, S.-I., Niwa, Y., O'Brien, K., Ono, T., Palmer, P. I., Pan, N., Pierrot, D., Pocock, K., Poulter, B., Resplandy, L., Robertson, E., Rödenbeck, C., Rodriguez, C., Rosan, T. M., Schwinger, J., Séférian, R., Shutler, J. D., Skjelvan, I., Steinhoff, T., Sun, Q., Sutton, A. J., Sweeney, C., Takao, S., Tanhua, T., Tans, P. P., Tian, X., Tian, H., Tilbrook, B., Tsujino, H., Tubiello, F., van der Werf, G. R., Walker, A. P., Wanninkhof, R., Whitehead, C., Willstrand Wranne, A., Wright, R., Yuan, W., Yue, C., Yue, X., Zaehle, S., Zeng, J., and Zheng, B.: Global Carbon Budget 2022, Earth System Science Data, 14, 4811–4900, https://doi.org/10.5194/essd-14-4811-2022, 2022.

Garnesson, P., Mangin, A., Fanton d'Andon O., Demaria, J., Bretagnon, M., The CMEMS GlobColour chlorophyll-a product based on satellite observation: multi-sensor merging and flagging strategies, Ocean Sci., 15, 819-830, Volume 15, issue 3, https://doi.org/10.5194/os-15-819-2019, 2019.

Good, S., Fiedler, E., Mao, C., Martin, M. J., Maycock, A., Reid, R., Roberts-Jones, J., Searle, T., Waters, J., While, J., and Worsfold, M.: The Current Configuration of the OSTIA System for Operational Production of Foundation Sea Surface Temperature and Ice Concentration Analyses, Remote Sensing, 12, https://www.mdpi.com/2072-4292/12/4/720, 2020.

Hersbach, H., Bell, B., Berrisford, P., Hirahara, S., Horányi, A., Muñoz-Sabater, J., Nicolas, J., Peubey, C., Radu, R., Schepers, D., Simmons, A., Soci, C., Abdalla, S., Abellan, X., Balsamo, G., Bechtold, P., Biavati, G., Bidlot, J., Bonavita, M., De Chiara, G., Dahlgren, P., Dee, D., Diamantakis, M., Dragani, R., Flemming, J., Forbes, R., Fuentes, M., Geer, A., Haimberger, L., Healy, S., Hogan, R. J., Hólm, E., Janisková, M., Keeley, S., Laloyaux, P., Lopez, P., Lupu, C., Radnoti, G., de Rosnay, P., Rozum, I., Vamborg, F., Villaume, S., and Thépaut, J.-N.: The ERA5 global reanalysis, Q. J. Roy. Meteor. Soc., 146, 19992049, https://doi.org/10.1002/qj.3803, 2020.

Ho, D. T., Law, C. S., Smith, M. J., Schlosser, P., Harvey, M., & Hill, P. (2006). Measurements of air-sea gas exchange at high wind speeds in the Southern Ocean: Implications for global parameterizations. Geophysical Research Letters, 33 (16). Retrieved 2019-06-25, from https://agupubs.onlinelibrary.wiley.com/doi/abs/10.1029/2006GL026817, doi: 10.1029/2006GL026817.

Körtzinger, A.: Determination of carbon dioxide partial pressure (pCO_2), edited by: Grasshoff, K., Kremling, K., and Ehrhardt, M., chap. 9, 149–158, John Wiley & Sons, Ltd, https://doi.org/10.1002/9783527613984.ch9, 1999.

Menemenlis, D., Campin, J., Heimbach, P., Hill, C., Lee, T., Nguyen, A., Schodlok, M., and Zhang, H.: ECCO2: High Resolution Global Ocean and Sea Ice Data Synthesis, 2008, OS31C-1292, 2008.

Naegler, T.: Reconciliation of excess 14C-constrained global CO_2 piston velocity estimates, Tellus B, 61, 372–384, 2009.

Pujol, M., Schaeffer, P., Faugère, Y., Raynal, M., Dibarboure, G., and Picot, N.: Gauging the Improvement of Recent Mean Sea Surface Models: A New Approach for Identifying and Quantifying Their Errors, J. Geophys. Res. Oceans, 123, 5889–5911, https://doi.org/10.1029/2017JC013503, 2018.

Pujol, M.-I., Faugère, Y., Taburet, G., Dupuy, S., Pelloquin, C., Ablain, M., and Picot, N.: DUACS DT2014: the new multi-mission altimeter data set reprocessed over 20years, Ocean Sci., 12, 1067–1090, https://doi.org/10.5194/os-12-1067-2016, 2016.

Regnier, P., Resplandy, L., Najjar, R. G., & Ciais, P. (2022). The land-to-ocean loops of the global carbon cycle. Nature, 603 (7901), 401–410.

Rödenbeck, C., Bakker, D. C. E., Gruber, N., Iida, Y., Jacobson, A. R., Jones, S., Landschützer, P., Metzl, N., Nakaoka, S., Olsen, A., Park, G.-H., Peylin, P., Rodgers, K. B., Sasse, T. P., Schuster, U., Shutler, J. D., Valsala, V., Wanninkhof, R., and Zeng, J.: Data-based estimates of the ocean carbon sink variability – first results of the Surface Ocean pCO_2 Mapping intercomparison (SOCOM), Biogeosciences, 12, 72517278, https://doi.org/10.5194/bg-12-7251-2015, 2015.

Takahashi, T., Sutherland, S. C., Wanninkhof, R., Sweeney, C., Feely, R. A., Chipman, D. W., Hales, B., Friederich, G., Chavez, F., Sabine, C., Watson, A., Bakker, D. C., Schuster, U., Metzl, N., Yoshikawa-Inoue, H., Ishii, M., Midorikawa, T., Nojiri, Y., Körtzinger, A., Steinhoff, T., Hoppema, M., Olafsson, J., Arnarson, T. S., Tilbrook, B., Johannessen, T., Olsen, A., Bellerby, R., Wong, C., Delille, B., Bates, N., and de Baar, H. J.: Climatological mean and decadal change in surface ocean pCO2, and net sea–air CO2 flux over the global oceans, Deep-Sea Res. Pt. 2, 56, 554–577, https://doi.org/10.1016/j.dsr2.2008.12.009, 2009.

Wang, X., Murtugudde, R., Hackert, E., Wang, J., and Beauchamp, J.: Seasonal to decadal variations of sea surface pCO_2 and sea-air CO_2 flux in the equatorial oceans over 1984–2013: A basin-scale comparison of the Pacific and Atlantic Oceans, Global Biogeochem. Cy., 29, 597–609, https://doi.org/10.1002/2014GB005031, 2015.

Wanninkhof, R.: Relationship between wind speed and gas exchange over the ocean revisited, Limnol. Oceanogr.-Meth., 12, 351–362, https://doi.org/10.4319/lom.2014.12.351, 2014.

Weiss, R.: Carbon dioxide in water and seawater: the solubility of a non-ideal gas, Mar. Chem., 2, 203–215, https://doi.org/10.1016/0304-4203(74)90015-2, 1974.

Zhang, Y., Xu, H., Qiao, F. *et al.* Seasonal variation of the global mixed layer depth: comparison between Argo data and FIO-ESM. *Front. Earth Sci.* 12, 24–36 (2018). https://doi.org/10.1007/s11707-017-0631-6